SECURITY CLASSIFICATION OF THIS PAGE (When Data Entered)

REPORT DOCUMENTATION PAGE		READ INSTRUCTIONS BEFORE COMPLETING FORM
1. REPORT NUMBER GRL/9601	2. GOVT ACCESSION NO.	3. RECIPIENT'S CATALOG NUMBER
4. TITLE (and Subtitle) BASIC STUDY OF THE PUMPING OF A GAMMA-RAY LASER		5. TYPE OF REPORT & PERIOD COVERED Final Report 03/15/93 - 03/14/96
		6. PERFORMING ORG. REPORT NUMBER
7. AUTHOR(s) C. B. Collins		8. CONTRACT OR GRANT NUMBER(s) N00014-93-K-2005
9. PERFORMING ORGANIZATION NAME AND ADDRESS University of Texas at Dallas Center for Quantum Electronics P.O. Box 830688 Richardson, TX 75083-0688		10. PROGRAM ELEMENT, PROJECT, TASK AREA & WORK UNIT NUMBERS
11. CONTROLLING OFFICE NAME AND ADDRESS Naval Research Laboratory 4555 Overlook Avenue, S.W. Washington, D.C. 20375-5000		12. REPORT DATE 04/15/96 13. NUMBER OF PAGES 81
14. MONITORING AGENCY NAME & ADDRESS(if different from Controlling Office) Dr. Paul Kepple Naval Research Laboratory 4555 Overlook Avenue, S.W. Washington, D.C. 20375-5000 Attn: Code 6721 Bldg. A50 Rm# 148		15. SECURITY CLASS. (of this report) Unclassified 15a. DECLASSIFICATION/DOWNGRADING SCHEDULE

16. DISTRIBUTION STATEMENT (of this Report)

This document has been approved for public release and sale; its distribution is unlimited.

17. DISTRIBUTION STATEMENT (of the abstract entered in Block 20, if different from Report)

18. SUPPLEMENTARY NOTES

19. KEY WORDS (Continue on reverse side if necessary and identify by block number)

Gamma-ray laser, Ultrashort wavelength laser

20. ABSTRACT (Continue on reverse side if necessary and identify by block number)

The most productive approaches to the problem of the gamma-ray laser have focused upon upconversion techniques in which metastable nuclei are pumped with long wavelength radiation. At the nuclear level the storage of energy can approach tera-Joules (10^{12}J) per liter for thousands of years. However, any plan to use such a resource for a gamma-ray laser poses problems of a broad interdisciplinary nature requiring the fusion of concepts taken from relatively unrelated fields of physics. Our research group has described
(continued on next page)

DISCLAIMER NOTICE

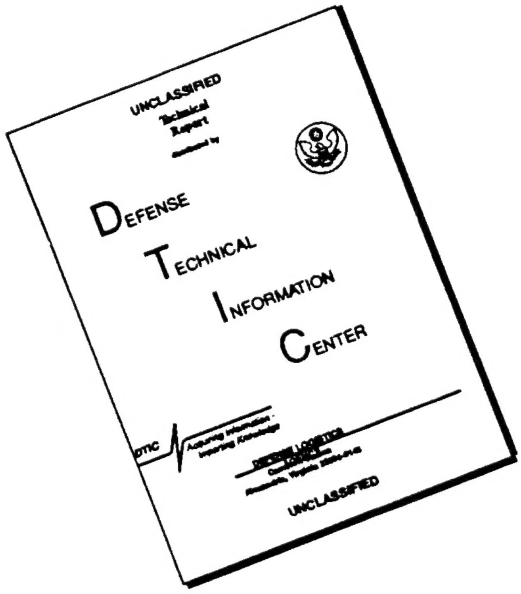

THIS DOCUMENT IS BEST QUALITY AVAILABLE. THE COPY FURNISHED TO DTIC CONTAINED A SIGNIFICANT NUMBER OF PAGES WHICH DO NOT REPRODUCE LEGIBLY.

I. Summary of Work Accomplished

I.1 Introduction

Many advanced technologies would benefit from non-nuclear sources of high energy density. The importance would be greatest if concentrated energies could be stored for long times and then released at controlled rates on time scales of nanoseconds to microseconds. For power released as electromagnetic waves, the archetypical system would probably be the laser, although many applications such as lithography need only the flash of "light" and not its coherence. In any event, gamma rays would represent the ultimate form for such "light."

Gamma rays are subject to the same basic laws governing the absorption and emission of electromagnetic radiation as prevail at longer wavelengths. However, since the energies per photon are so much greater, there seem to be singular advantages in gamma-ray analogs of atomic and molecular sources for the production of intense pulses of "light." Such perceptions have driven the 36 year quest for the ultimate pulsed-power device, ***the gamma-ray laser.*** In fact, the advantages accrue more from the higher densities for the storage of energy than from the shorter wavelengths available upon release. A flash of induced emission at gamma-ray wavelengths would be of great technological importance in its own right, while at the same time demonstrating the means for pumping a gamma-ray laser.

Any grouping of electrically charged particles can radiate electromagnetic waves with the characteristic size of the charge distribution generally determining the type of photons most efficiently emitted. Antennas emit radio waves, waveguide structures emit microwaves, electrons oscillating against the positive nuclei in atoms emit optical light and x rays, and protons and neutrons moving in nuclei emit gamma rays. Once emitted, gamma rays are no different than x rays which often have the same energies. Since the oscillating charges in the

nucleus emit their energy as short-wavelength electromagnetic waves ***this process is not a nuclear reaction.*** None of the interior particles are emitted to cause a nuclear reaction and the nucleus finishes as the stable (non-radioactive) ground state of the same isotope of the same element.

The nucleus is the smallest part of an atom which in turn is the smallest structural unit of physical matter. Thus, quantum mechanics teaches that the motions of the charged particles found within the nucleus will represent the highest velocities of circulation possible in a sample of any material. This fundamental precept means that the very highest densities of (non-nuclear) energy storage will be found in the motions of those charges. Just as in the case of atoms, the movement of charges in a nucleus can absorb photons of electromagnetic waves, which in this case are x rays, and make a transition to an excited state of higher energy. Because of the high energy densities and great velocities, the charges usually reradiate such energies in times too short to be measured ($< 10^{-18}$ s.) However, in rare cases selection rules sufficiently inhibit the coupling of the particle motion to the electromagnetic field for the energies to be stored for tens and even thousands of years in those special nuclei. Such long-lived (metastable), high-energy states of excitation are termed isomeric levels and the materials are simply known as isomers. Such isomers are natural sources of high energy densities.

Our research on the gamma-ray laser identified 29 outstanding isomers which store exceptionally high densities of energy. Four examples are cited in Table I; to appreciate the energy densities presented there it should be noted that a μg of material is comparable to the amount of ink used to print a period at the end of a sentence. It can be seen that the energy storage of the best of the isomers, $^{178}Hf^{m2}$ is more than a gigajoule per gram. Since one of its key transitions for the output of electromagnetic radiation has a lifetime of 70 ns after triggering,

the power density available from that material is (1.3×10^9 J g^{-1} / 7×10^{-8} s), or about ***0.05 exawatt per gram.***

Since isomers derive their long shelf lives from their poor coupling to electromagnetic waves, it was traditionally thought to be impossible to trigger the release of the stored energy. However, a recent and major breakthrough in research on the feasibility of a gamma-ray laser showed the existence of a giant pumping resonance at an energy near 2.5 MeV in nuclei with masses around 180. In effect, this resonance provided a "gateway" state through which the selection rules making an isomer long-lived could be violated. If an isomeric level initially stored an energy of 2.0 MeV, only 0.5 MeV would be needed to reach a gateway at 2.5 MeV. The absorption of an x-ray photon of that energy would excite the system to such a level which would be very strongly coupled to the electromagnetic fields. The sum of the stored energy and that of the trigger x-ray photon would then be promptly emitted, or dumped, as gamma rays.

The concept for dumping the energy from controlled fractions of isomeric populations has been demonstrated in a series of experiments with the fourth of the materials listed in Table I. This was first accomplished in the Center for Quantum Electronics at the University of Texas at Dallas (UTD) and was subsequently confirmed in separate experiments at the Institut für Kernphysik, Technische Hochschule Darmstadt. The systematics for the occurrence of the giant pumping resonances has been proven in a series of UTD experiments which located them in nuclei in the region of masses between 167 and 195.

The triggered release of stored energy into electromagnetic waves works and works well. The pervasive problem has been that of the 29 promising materials, only two have yet been available for study. The production of this type of ultrahigh energy density materials is still in its infancy, although remarkable progress has already been made. For example, more than 10^{16} nuclei of the best of the materials, $^{178}Hf^{m2}$ are already available. Although not yet mass-

separated and carrier free, this is an amount from which it should be possible to obtain a target containing more that 10^{15} nuclei with essentially 100% inversion for future experiments.

It would be the very best of all possibilities to be able to immediately realize the release of high energy densities into a ***coherent*** radiation field. However, simply the induced emission of gamma rays from an isomeric sample at such powers would be of considerable technological significance. That goal is close at hand. Once attained, the development of increasing levels of coherence can be approached as a next logical objective. The triggering of the gamma radiation has been the object of our research as a first step in the pumping of a gamma-ray laser.

I.2 Technical Background

I.2.1 History

Research on the development of a gamma-ray laser has followed a cyclical pattern over the past 36 years with a marked abundance of concepts and approaches. Because of the complex branching of approaches it is often difficult to follow the development of a particular idea in order to properly recognize the brilliance of the early work. However, the origins are perfectly clear. The original proposal for a gamma-ray laser was made by the distinguished Russian Professor Lev Rivlin in 1961 [1]. It went largely unnoticed at the time and the first cycle of research on this topic developed a strong momentum two years later as a result of independent early publications from the US [2,3] and Russia [4,5].

In the first cycle of study which lasted from 1963 - 1980, considerable attention was given to the problem of suddenly assembling a critical density of prepumped nuclei to reach the threshold for stimulated emission. At the end of this period it was generally accepted that such brute force approaches, usually requiring *in situ* pumping and involving only a single (output) photon, were essentially hopeless. In an encyclopedic review, Baldwin and coauthors [6]

concluded the general impossibility of a gamma-ray laser based upon all techniques for pumping known in 1980. That review effectively documented the failure of the traditional approaches to a gamma-ray laser, those relying on the use of intense particle fluxes for input energy. However, toward the end of the first cycle of research the precursors of a new interdisciplinary concept began to appear [7-13]. Based upon nuclear analogs of quantum electronics, these "optical" approaches developed rapidly and launched a renaissance in the field. The basic theory [14-16] of upconversion at the nuclear level was in place by 1982 for the two possible variants, coherent and incoherent upconversion. The use of either multiphoton processes or multiple electromagnetic transitions to release the energy stored in isomers avoided many of the difficulties encountered with more traditional pumping schemes.

Since 1980, research on the feasibility of a gamma-ray laser has taken on a completely new character. In the first half decade a series of experiments verified that the concepts of quantum electronics could be applied at the nuclear level [17-21]. By 1986 one blueprint for a gamma-ray laser [16] had been established and a substantial effort was initiated toward the demonstration of its feasibility. In the past decade major advances have resulted from US research, first supported by SDIO and then by BMDO through NRL. Those advances have significantly increased the likelihood of the feasibility of a gamma-ray laser while demonstrating the means for the induced emission of gamma radiation.

I.2.2 Concepts

At first approach it would seem that the prospects for all ultrashort-wavelength lasers would be vitiated by a very fundamental factor [6]. The basic ν^3 dependence of electron transition probabilities upon frequency, ν so limits the storage of pump energies in atoms and molecules that even now some of the largest pulsed-power machines are able to excite only milliJoules of laser output and then only at soft x-ray energies. In contrast there are four unique advantages of a gamma-ray laser that would accrue from its operation upon electromagnetic transitions of nuclei:

1) The constant linking ν^3 with lifetime is more favorable by orders-of-magnitude because of the accessibility of a variety of transition moments. The effects pumped by an input pulse can be integrated up to larger values for longer times.

2) Nuclear metastables store keV and even MeV for years. With upconversion schemes most of the energy is input *ex situ*, long before the time of use and triggering requirements are small.

3) Nuclear transitions need not experience thermal broadening and natural linewidths are routinely obtained. Without broadening, electromagnetic cross sections are large and values for 1 Å transitions typically exceed the cross section for the stimulation of Nd in YAG.

4) Working metastables can be concentrated to solid densities.

The essential concept driving the renaissance in gamma-ray laser research was the "optical" pumping of nuclei [7-16]. In this context optical meant x rays, but the fundamentals were the same. Useful, resonant absorption of pump power would occur over short distances in a thin low-Z medium to produce high concentrations of excited nuclei while wasted wavelengths would only be degraded to heat in much larger volumes. This was the basic

concept for avoiding the severe material damage which would have destroyed the Mössbauer effect that would have resulted from the particle-pumping schemes of the first cycle of research emphasized before 1980. In the blueprint of 1982 for upconversions [16], one of several possible types of resonant photopumping was envisioned to transfer the stored population of an isomer to a "gateway" state at the head of a cascade leading to the upper laser level. Of the cases considered, this nuclear analog of the ruby laser embodied the simplest concepts for a gamma-ray laser. Not surprisingly, the greatest rate of achievement in the last decade in the pumping of high-energy density media has been realized in that direction.

For ruby, the identification and exploitation of a bandwidth funnel were the critical keys in the development of the first laser. There was a broad absorption band linked through efficient cascading to the narrow laser level. Our theory [16] called for a nuclear analog of this structure which was unknown in 1986 when intensive experiments were started. Now, that theory has been confirmed.

I.2.3 Theoretical Model

The sequence for triggering the release of the energy stored in an isomeric state [16,22] is shown in Fig. 1. The population in the initial level is transferred to a broad pump band, or "gateway" state, which bridges the selection rules that would otherwise limit the coupling of the isomer to the electromagnetic fields. The normal decay from the gateway is accompanied by the emission of immediate fluorescence and leads to the principal laser level from which the sustained output of power will be emitted. Population can be accumulated in that level by continuing to run the pump cycle for a time comparable to the lifetime of the output state.

Pumping processes like that of Fig. 1 have been known for over 50 years [23,24] although relatively few results have been published in that time. Practical difficulties with the calibration and availability of sources of irradiation had limited the degree of reproducibility

achieved in work prior to about 1987, as discussed in the next section. The processes are classified as inelastic scattering, or (γ,γ'), reactions in the literature of nuclear physics where the γ and γ' represent the incident and scattered photons, respectively. In terms of the target nucleus, X the notation is $X(\gamma,\gamma')X^*$ in which X^* represents the same nucleus in its final state of excitation. If the final state is an isomer, the * is replaced by m.

For a sample that is optically thin at the pump wavelength, a computation of the number of nuclei pumped by a (γ,γ') reaction into a given excited state should be straightforward [16,22,25]. Most intense x-ray sources emit continua, either because bremsstrahlung is initially produced or because spectral lines are degraded by Compton scattering in the immediate environment. Then the irradiation of a sample containing N_i target nuclei in the initial state results in a time-integrated yield of final-state nuclei, N_f according to the general relation

$$N_f = N_i \Phi_0 \int_0^{E_0} \sigma(E)\, F(E, E_0)\, dE \quad , \qquad (1)$$

where the photoexcitation reaction is described by the energy-dependent cross section, $\sigma(E)$. The photon continuum is represented by an endpoint, E_0 and the time-integrated spectral intensity, ϕ which is written as the product of the total x-ray flux incident on the sample, Φ_0 in photons cm^{-2}, and a function $F(E,E_0)$ that gives the distribution of intensities within the continuum. The distribution is normalized so that

$$\int_0^{E_0} F(E, E_0)\, dE = 1 \quad . \qquad (2)$$

All (γ,γ') reactions occurring at energies below the threshold for particle evaporation resonantly excite discrete levels [25,26]; for the population of isomers the relevant levels are

pump bands like that depicted in Fig. 1. Only one gateway appears there, but there could be more. Each gateway, identified by the index j, would be excited at a different energy, E_j but all would branch to some extent into the same fluorescent final state, f. Although the width of the j-th level is broad on a nuclear scale, it is narrow in comparison to the scale of energies, E over which $F(E,E_0)$ varies. Thus, the final-state yield can be written from Eq. (1) as

$$A_f(E_0) \equiv \frac{N_f}{N_i \Phi_0} = \sum_j (\sigma\Gamma)_{fj} \, F(E_j, E_0) \quad , \tag{3}$$

where the activation, $A_f(E_0)$ has been introduced. This quantity is the fractional yield of the final state, f normalized per unit photon flux in the irradiating continuum. The summation in Eq. (3) extends over all gateways whose excitation energies are less than the endpoint. In this expression $(\sigma\Gamma)_{fj}$ is the integrated cross section for the production of the final-state population, N_f as a result of excitation through the gateway at E_j, so that

$$(\sigma\Gamma)_{fj} = \int_{E_j-\Delta}^{E_j+\Delta} \sigma(E)\, dE \quad , \tag{4}$$

where Δ is an energy small compared to the spacing between gateways but large in comparison to their widths. For each gateway the integration is performed over a Lorentzian line shape which for a purely radiative transition has the natural width, $\Gamma = (\hbar \ln 2)/T_{1/2}$, with $T_{1/2}$ being its halflife. It is straightforward to show that

$$(\sigma\Gamma)_{fj} = (\pi b_a b_o \Gamma \sigma_0/2)_{fj} \quad , \tag{5}$$

in which the branching ratios b_a and b_o specify the probabilities that a population pumped by absorption into the j-th gateway will decay back into the initial state or by cascade to the output

level, respectively. The quantity $\sigma_0/2$ is the peak of the Breit-Wigner cross section [25,27] for the absorption transition,

$$\sigma_0 = \frac{\lambda^2}{2\pi} \frac{2I_j+1}{2I_g+1} \frac{1}{\alpha_p+1} \quad . \tag{6}$$

where λ is the wavelength of the x ray at the resonant pump energy, E_j, the angular momenta of the gateway and ground states are I_j and I_g, respectively, and α_p is the total internal conversion coefficient for the pump step shown in Fig. 1.

Whether or not the initial state being pumped is the ground state or a long-lived isomeric level, the principal figure of merit is the integrated cross section. This quantity reflects the efficacy for the transfer of population to a fluorescence level, and therefore available to an output transition. Thus, it is the nuclear equivalent of the fluorescence efficiency so important in the early development of atomic and molecular lasers.

I.3. Critical Experiments

I.3.1 Foundations

I.3.1.1 Model Verification

The most tractable (γ,γ') reactions for study are those for the photoexcitation of stable isotopes from their ground states up to isomeric levels. In many cases the product is sufficiently long-lived to be readily examined after termination of the input irradiation although lessons can be learned that can be applied to excitation of the shorter-lived levels more useful in a laser. The prototype for basic study has been the reaction $^{111}Cd(\gamma,\gamma')^{111}Cd^m$ exciting the 48.6 min level at 396 keV. Three of the classical measurements of integrated cross section were conducted in 1979, 1982, and 1986 as reported in Refs. [28-30], respectively. Probable errors were quoted

as varying only from 7 to 14%, and yet no two of the measurements were even within a factor of 2 of each other. This discrepancy led to serious contentions over the way in which the expected fluorescence yields were calculated [29]. Because of the pervasive disagreements in the literature about nuclear photopumping, one of the first priorities in the most recent cycle of research was placed upon quantitative validation of the model.

Many of the early conflicting measurements were performed with the use of radioisotopes for the irradiation of samples. From the perspective of laser physics, those would appear to be the most unreliable sources of energetic photons for (γ,γ') reaction studies. Although assumed to emit line spectra, in actual usage they produced intensities which were dominated by continua resulting from photons which had sustained multiple Compton scattering by collimators and shielding in the irradiation environment. Such multiple scatterings are difficult to calculate and are still impossible to measure in practical laboratory configurations without further perturbing the spectra. In contrast, the spectral intensities of bremsstrahlung are routinely calculated with high accuracy from measured accelerator currents and target geometries by well-established, modern computer codes [31,32] such as are commonly used in radiological treatment planning [33].

In our experimental work of the last five years the bremsstrahlung from six accelerators in different experimental environments was used to verify the fluorescence model of Eqs. (1) - (6) and to cross-check the accelerator intensities. The devices involved in this effort were the e-beam machines DNA/PITHON at Physics International and DNA/Aurora at the US Army Research Laboratory, a 4 MeV and a 6 MeV medical linac at the University of Texas Health Sciences Center, the superconducting injector to the storage ring at Darmstadt (S-DALINAC) and our own 4 MeV linac, the Texas-X. Spectral intensities from bremsstrahlung targets irradiated by these accelerators were calculated with the EGS4 coupled electron/photon transport

code [31] for the linacs and with the TIGER code [32] for the e-beam devices. The codes were adapted for each individual configuration and closely monitored values of electron currents were used as inputs to the calculations. In this way both $F(E,E_0)$ and Φ_0 were obtained. In some instances Φ_0 was separately verified by in-line dosimetry using thermoluminescent dosimeters (TLD's) or ionization chambers.

Of the many potential nuclides which might be used to confirm the formulations of Eqs. (1) - (6), the early literature [34] supported the calculation of integrated cross sections for very few. Table II includes those which were known with sufficient accuracy to serve as standards. In the convenient units of 10^{-29} cm^2 keV, values of integrated cross section ranging from the order of unity to a few tens characterize bandwidth funnels that are sufficient for demonstrations of nuclear fluorescence from reasonable amounts of material at readily accessible levels of input.

In the calibration experiments, samples with typical masses of grams were exposed to the bremsstrahlung from the six accelerators for times ranging from seconds to hours for the continuously operating machines and to single flashes from the pulsed devices. The activations, A_f of Eq. (3) were determined by counting the photons spontaneously emitted from the samples after transferring them from an accelerator chamber to a quieter environment. Usual corrections were made for the isotopic abundance, for the loss of activity during irradiation and transit, for the counting geometry, for the self absorption of the fluorescence, and for the tabulated efficiencies [35] for the emission of signature photons from the populations, N_f. The self absorption factor required a calculation of photon transport within the target materials which was verified in some cases by confirming that the same sample masses in different geometries with different correction factors gave the same final populations.

Measured results were in close agreement [36] with the predictions of Eq. (3) using the values of $(\sigma\Gamma)_{fj}$ given in Table II. A typical example for the reaction $^{87}Sr(\gamma,\gamma')^{87}Sr^m$ is shown

in Fig. 2b in which the plot of activation against bremsstrahlung endpoint gives its "excitation function" [37]. Particularly valuable were the data [38] obtained with the S-DALINAC because of its ability to continuously vary the endpoint. A change of E_0, as well as altering Φ_0, modulates the spectral distribution function, $F(E_j,E_0)$ at all of the important energies for resonant excitation, E_j. The largest effect occurs when E_0 is increased from a value just below a gateway to one exceeding it so that $F(E_j,E_0)$ varies from zero to some finite value as depicted in Fig. 2a.

Early work [39,40] on (γ,γ') reactions had shown that excitation functions displayed very pronounced "activation edges" at the resonant excitation energies, E_j of gateways. Such activation edges are clearly seen in the data of Fig. 2b. There is excellent agreement between measurements obtained with the different accelerators, and between the experimental data and the model calculations made using the literature values [38,39] of Table II. It is useful to note that the units of A_f are those of area because they are a type of average cross section quite different from the σ_0 of Eq. (6) that describes an individual transition. The small ordinate values are due to the normalization of Eq. (3) which effectively averages the large σ_0 at the resonant energy, E_j over the broad bandwidth of the entire irradiating continuum, within which most $E \neq E_j$.

I.3.1.2 Pump Calibration

The high level of agreement between the measurements and the model established a confidence level sufficient to support the use of (γ,γ') reactions which populate isomers as a means of selectively sampling the spectra of single x-ray pulses like those from e-beam devices. This technique of x-ray activation of nuclei (XAN) directly measures absolute intensities at discrete energies corresponding to the E_j of gateways accessible to the bremsstrahlung [36,41-44]. An example of an XAN calibration is shown in Fig. 3 for the spectrum from a single shot at an endpoint of 1.4 MeV from DNA/PITHON [42]. No scaling was involved and absolute

intensities were obtained using Eq. (3), integrated cross sections from Table II, measured masses of the samples, the distances, and the activations produced. Having calibrated the spectral sources used in these experiments, the persisting uncertainties in the optical pumping of $^{115}In^{m}$ and $^{111}Cd^{m}$ were resolved [45,46] as being primarily due to the use of radioisotopes as sources of irradiation [26].

Following the further improvements in the nuclear data base listed in Table II, it has been possible to extend the XAN procedure to span the range to 4 MeV [47,48]. Figure 4 shows an example of direct measurements [47] of the spectral intensity from a 4 MeV linac using the nuclear standards from Table II in comparison with the calculated bremsstrahlung output.

These calibration studies served to confirm both the traditional model of nuclear activation summarized in Eqs. (1) - (6) and to validate the computer codes for calculating bremsstrahlung intensities based on measured accelerator parameters. ***Now, there can be no reasonable doubt of procedures for quantitatively measuring integrated cross sections if an experiment is carefully performed with a bremsstrahlung source of pump radiation.***

I.3.1.3 Limits on Spurious Contributions

Sources of possible spurious contaminations of the measurements were carefully considered. Those could have included contributions to the isomeric yield from natural background or excitation of the samples by (e,e'), (γ,n), (n,γ) or (n,n') reactions. In the case of natural background, positive identification of the fluorescence signatures and the amounts of yields was accomplished by obtaining both energy (pulse-height) and decay (multichannel scalar) spectra. Typical examples [49] are shown in Figs. 5 and 6 for the isomers of $^{167}Er^{m}$ and $^{123}Te^{m}$. As can be seen in those figures, excellent agreement was obtained between the measured halflives and the literature values [35] of 2.28 s and 123 days, respectively. Fluorescence signatures were clearly identified and were well-separated from any strong background lines when either NaI(Tl) or HPGe detectors were used.

Inelastic electron scattering, or (e,e'), reactions can excite isomeric populations in a manner that at low momentum transfer is quite similar to that of (γ,γ') reactions [50]. However, it has been experimentally demonstrated [39] that the cross sections for electro-excitation of isomers are on the order of 10^2 smaller than for photoexcitation at the same energy. The numbers of electrons available for (e,e') reactions after penetrating the high-Z bremsstrahlung converters are also orders-of-magnitude less than the numbers of x rays produced. An example of a typical converter is the 3-mm thick tantalum target used in irradiations with the Texas-X, within which the range of 4 MeV electrons was only 1.7 mm. Spurious contributions to the measured activations due to (e,e') reactions were therefore negligible. Likewise, contaminations from (γ,n) reactions could be summarily excluded since photons within the bremsstrahlung had insufficient energy [34] to reach the thresholds for those processes in the sample materials except in the very highest energy irradiations with DNA/Aurora.

The question of spurious contributions from (n,γ) or (n,n') reactions received more consideration. All of the accelerators used, other than DNA/PITHON, were capable of evaporating neutrons from some materials in the accelerator environments. Thus, it was important to determine the amount of isomeric yield which could have been attributed to neutrons. This was done in four separate studies [38,47,48,51] published in 1990 - 1993. The largest contribution was found for experiments conducted with the 6 MeV medical linac where neutrons produced from a Be window could have given as much as an additional 6% to the activation yield [49]. In contrast, our 4 MeV Texas-X, built especially to minimize the amounts of Be and cooling water exposed to the irradiation, held neutron contributions [47] to less than 0.001%. Even though the extent of contamination by neutron contributions was negligible in all experiments conducted, the diagnostic procedures used to verify this point are reviewed here for convenience.

In principle, the two types of neutron reactions that had to be considered were inelastic (n,n') reactions which would have required hot neutrons and neutron capture (n,γ) processes driven by fluxes of thermal or epithermal neutrons. Contributions from the latter were directly determined in accordance with standard procedures [52]. The thermal neutron fluxes were measured by irradiating pairs of thin indium foils, one bare and the other shielded within a cadmium cover. Energy spectra obtained from these foils were examined after exposure for fluorescence from the isomer $^{116}In^{m}$, which is produced by a branch of the reaction $^{115}In(n,\gamma)^{116}In^{m,g}$. The magnitudes of the fluorescence lines observed in both the bare and the shielded samples allowed the determination of the thermal neutron flux which was 12 neutrons cm^{-2} s^{-1} in the worst case of the 6 MeV linac environment. The contributions to the activations from thermal neutrons are reported in the literature for all nuclides studied [49] and in all cases were small.

In reduced-Be accelerators like the Texas-X, fast neutrons primarily arise from the photodissociation of the deuterium fraction in the cooling water, the humidity of the air, and the concrete used in construction. It is useful to recall that the production of significant fluxes of fast neutrons is unlikely, *a priori*, because the dissociation energy of deuterium is 2.22 MeV. For a bremsstrahlung endpoint of 4 MeV, this leaves only a maximum of 0.89 MeV kinetic energy for each of the resulting proton and neutron. Those must recede at right angles from the path of the incident photon in order to conserve momentum. Nevertheless, one might assume there to be a large mass of deuterium geometrically placed at right angles to the line-of-sight between the bremsstrahlung target and the sample being illuminated. This would enable the primary neutrons carrying the full 0.89 MeV to irradiate the material under study and they might contribute to the excitation. However, cross sections [53] for inelastic excitation by 1-MeV neutrons rarely exceed 1b so the probable impact parameter can be readily bounded and it can be concluded that only s-wave, p-wave, and perhaps d-wave scattering are probable. In the cases of most isomers, the angular momentum and its projections between initial and final states differ by more than two units so excitation by fast neutrons must confront the same difficulties encountered by photoexcitation. Moreover, only levels lying below 0.89 MeV can be accessed where there is a paucity of gateway states. Photoexcitation with 4 MeV bremsstrahlung can access pump levels up to 4 MeV, *so photoneutrons present no natural advantages in exciting high-multipolarity transitions, even assuming the unlikely geometry needed to produce large numbers of those particles.*

Notwithstanding the lack of a credible rationale for concern about the possible contamination of yields by (n,n') reactions, measurements were made of the fast neutron flux at the position of the irradiated targets using standard techniques [54]. Samples were covered with foils containing ^{46}Ti, ^{47}Ti, and ^{58}Ni, nuclides having large cross sections for (n,p) reactions

at energies in the relevant range. No fluorescence was detected to indicate product nuclei and measurements were completely negative in all photoexcitation experiments [53]. Calculations of the expected flux of fast neutrons from the environment were consistent with this negative, predicting effects orders-of-magnitude below the threshold of detection. The possibility of fast-neutron contributions was further examined by covering samples used in the (γ,γ') studies with a planchette containing heavy water, D_2O to enhance the prevalence of photodissociation neutrons. Still no increase was observed in isomeric yields, in complete agreement with computations. Photoneutron production from other potential sources such as photodissociation of O_2 in the air was also found to be unimportant [53].

All of these negatives for (n,n') contributions were consistent with the successes in reproducing the absolute measurements of the calibration (γ,γ') reactions known from the literature [34] with so many different accelerators having such a variety of windows, cooling geometries, and physical enclosures. The contamination of (γ,γ') reaction yields by (n,n') reactions was assuredly undetectable in comparison to possible contributions from (n,γ) reactions which could have been as large as 0.1% in typical cases and 6% in the worst case [47,49,51] given the measured values of neutron flux and neutron cross sections. Overall, spurious contributions to the measured activations due to natural background and incidental (e,e'), (γ,n), (n,γ) and (n,n') reactions were found to be negligible.

I.3.2 Giant Pumping Resonances

I.3.2.1 Discovery

Expressed as partial widths, $b_a b_o \Gamma$, the integrated cross sections for the excitation of $^{77}Se^m$, $^{79}Br^m$, and $^{115}In^m$ seen in Table II correspond to 39, 5, and 94 μeV, respectively. While among the largest values reported prior to our studies, these results still left an aura of credibility to the traditional impressions that partial widths for exciting isomers would be limited to about 1 μeV.

Tempering expectations that integrated cross sections of even the magnitudes of Table II might be expected for the dumping of actual isomeric candidates for a gamma-ray laser was a concern for the conservation of various projections of the angular momenta of the nuclei. Many of the interesting candidate isomers belong to the class of nuclei deformed from the normally spherical shape. For those nuclides there is an additional quantum number of dominant importance, K which is the projection of individual nucleonic angular momenta upon the axis of elongation. To this is added the collective rotation of the nucleus to obtain the total angular momentum, J. The resulting system of energy levels resembles that of a diatomic molecule for which

$$E_n(K,J) = E_n(K) + B_n J(J+1) \quad , \qquad (7)$$

where $J \geq K \geq 0$ and J takes the values $|K|$, $|K| + 1$, $|K| + 2$,.... In this expression B_n is a rotational constant that is inversely proportional to the nuclear moment of inertia, and $E_n(K)$ is the lowest value for any level in the resulting "band" of energies identified by other quantum numbers, n. That level is termed the "bandhead." The selection rules for electromagnetic transitions then require both $|\Delta J| \leq M$ and $|\Delta K| \leq M$, where M is the multipolarity of the

transition. In most cases an isomeric state has a large lifetime because it lies in a band whose value of K differs considerably from those of lower levels to which it would otherwise be radiatively connected. As a consequence, bandwidth funneling processes such as shown in Fig. 1 that start from isomeric levels must span substantial changes in K and component transitions have been expected to have large, and hence unlikely, multipolarities.

From this perspective the candidate isomer, $^{180}Ta^{m}$ was the most initially unattractive as it had the largest difference in K between isomer and ground state, 8ħ. However, because a macroscopic sample was readily available, $^{180}Ta^{m}$ became the first isomeric material to be optically pumped to a fluorescent level. This particular nuclide carries a dual distinction. It is the rarest stable isotope occurring in nature [35] and it is the only naturally occurring isomer. The ground state of ^{180}Ta is 1^{+} with a halflife of 8.1 hours while the tantalum nucleus of mass 180 occurring with 0.012% natural abundance is actually the 9^{-} isomer, $^{180}Ta^{m}$. It has an adopted excitation energy of 75.3 keV and a halflife in excess of 1.2×10^{15} years.

In an experiment conducted in 1987, 1.2 mg of $^{180}Ta^{m}$ was exposed to bremsstrahlung and a large fluorescence yield was obtained [55]. This was the first time a (γ,γ') reaction had been excited from an isomeric target as needed for a gamma-ray laser and was the first evidence of the existence of giant pumping resonances. Simply the observation of fluorescence from a milligram-sized target proved that an unexpectedly large reaction channel had opened. Usually grams of material had been required in this type of experiment [49].

The energy-level diagram of ^{180}Ta and its daughters [34] is shown in Fig. 7, together with a schematic representation of the individual steps in the excitation and detection of the $^{180}Ta^{m}(\gamma,\gamma')^{180}Ta$ reaction. As can be seen in the figure, the principal means for the detection of the ^{180}Ta ground state lies in observing the K_{α} lines of its daughter ^{180}Hf, produced by electron capture decay. The efficiency for the emission of K_{α} photons relative to the number of ^{180}Ta

decays is about 57% [35]. The target used in these experiments was enriched to contain 1.2 mg of ^{180}Ta diluted in 24.7 mg of ^{181}Ta. Deposited as a dusting of oxide near the center of the surface of a 5-cm disk of Al and overcoated with a 0.25 mm layer of Kapton, this sample was believed to be free from self absorption of the x rays from the daughter Hf. Such a construction minimized corrections to the raw data and since self absorption was neglected, the final results could only underestimate the activation had there been some unexpected absorption.

The sample was exposed to bremsstrahlung from the 6 MeV medical linac whose output dose rate had been calibrated with an accuracy of $\pm$ 3%. This was the machine that presented the worst-case neutron flux which could have contributed another 6% error. However, as described below, the measurements were subsequently confirmed in absolute comparisons with data taken at the S-DALINAC. After the irradiation, the sample was counted with an n-type, HPGe spectrometer. Conventional techniques were used to calibrate the counting system with isotopic standards. Figure 8 shows the spectra from the enriched target before and after a 4-h, 6-MeV irradiation, while Fig. 9 shows the dependence upon time of the counting rate observed in the Hf(K_α) peaks after the exposure. Data points are plotted at the particular times at which the instantaneous counting rate equals the average counting rate measured over the finite time intervals shown. The figure shows the close agreement between the measured decay and the literature value for the ground-state halflife of 8.1 h. Analyses [38,55] of the data indicated that the partial width for the dumping of ^{180}Ta^{m} was around 0.5 eV.

To determine the transition energy, E_j from the ^{180}Ta^{m} isomer to the gateway level, a series of irradiations [38] was made at the S-DALINAC facility using fourteen different endpoints in the range from 2.0 to 6.0 MeV. The existence of an activation edge was clearly seen in the data shown in Fig. 10b. The fitting of such data to the expression of Eq. (3) by adjusting trial values of $(\sigma\Gamma)_{fj}$ provided the integrated cross sections for the dumping of ^{180}Ta^{m}

isomeric populations into freely radiating states. Reported values [38] are summarized in Table III and shown schematically in Fig. 10a. The lowest-lying giant pumping resonance was found at an excitation energy near 2.8 MeV.

The integrated cross sections in Table III are enormous values exceeding anything previously reported for transfer through a bandwidth funnel by two orders-of-magnitude. In fact they are 10,000 times larger than the values usually measured for (γ,γ') reactions in nuclei.

I.3.2.2 Systematics

A survey of 19 isotopes [49] conducted with the four U.S. accelerators over a fairly coarse mesh of bremsstrahlung endpoints confirmed the existence of giant resonances for the photoexcitation of isomers in the region of masses near 180. A summary of the results is shown in Fig. 11. Activation edges observed in excitation functions measured [56] using the S-DALINAC continued to support the identifications of integrated cross sections for pumping and dumping of isomers in the mass-180 region that were on the order of 10,000 times greater than usual values. Another study [51] with the S-DALINAC showed that the giant pumping resonances reappeared at lower masses near 120. The close similarity seen in Fig. 11 for integrated cross sections and excitation energies for gateways between nuclei with such dissimilar single-particle structures seems to support the identification of the giant pumping resonances with some type of property of the nuclear core. Whatever the mechanisms, the experimental fact remains that interband transfer processes connecting isomers to freely-radiating levels can almost commonly be pumped through enormous partial widths reaching 0.5 eV, even when the transfer of angular momentum must be as great as $\Delta K = 8$. It seems this is the nuclear analog of the giant resonance for pumping ruby at the atomic level.

I.3.2.3 Structure

As encouraging as were the studies showing the frequency with which giant pumping resonances occurred throughout the table of nuclides, a major concern remained. To lower pump requirements for a laser it is necessary that the $(\sigma\Gamma)$ be large, but this alone is not sufficient. In the ideal case [57] the integrated cross section would be elevated by a strong width multiplying a cross section for absorption having the maximum value possible from Eq. (6). In that case the ratio of pump power per unit volume absorbed resonantly to excite nuclei to the fraction absorbed nonresonantly and degraded to heat would be the largest possible. This is an important factor in thermal survival.

The density of excited states is very high in the nuclei favored in Fig. 11, and is especially so in ^{180}Ta because it is one of the few stable odd-odd nuclei. It could have been the case that the remarkable magnitude found for $(\sigma\Gamma)$ in the dumping of the population of $^{180}Ta^{m}$ was the result of a great number of adjacent gateways with $(\sigma\Gamma)_{fj}$ of unremarkable size, but adding in Eq. (3) to give a surprising total yield. While such a result would have still been exciting, it would have been much less helpful in rejecting the waste pump power degraded to heat. To show that this was not the case required that scattering measurements be performed.

From Fig. 1 it can be seen that photoexcitation events which do not lead to the population of the state f should be detected by the reemission, or elastic scattering, of the incident photon initially absorbed by the gateway. In analogy with the $(\sigma\Gamma)_{fj}$ of Eq. (5), the integrated cross section for scattering can be written,

$$(\sigma\Gamma)_{0j} = (\pi b_a^2 \Gamma \sigma_0 / 2)_{0j} \quad . \tag{8}$$

A large value of $(\sigma\Gamma)_{0j}$ would insure that enough photons could be scattered for spectroscopic analysis to determine at what energies the corresponding transitions were excited. In the event

$b_a < 1$, some fraction of the gateway-state population would also decay to the isomer to contribute to $(\sigma\Gamma)_{fj}$ and the energies for excitation of some of the giant pumping resonances could be accurately determined.

The design of an experiment to compliment activation measurements by identifying scattering from the pumping resonances requires a nuclide with several favorable properties. It must have an isomer with a reasonable lifetime of seconds to hours and be available in gram quantities with isotopic purity. Beyond such practical concerns would be the desire to have the nuclear structure well-characterized for energies below those at which giant pumping resonances would be expected. With these constraints it was relatively straightforward to identify ^{115}In as an optimal vehicle for a first test.

A modern experimental arrangement especially designed for nuclear resonance fluorescence (NRF) experiments has been recently described [58]. The spectrum of the intense bremsstrahlung produced by the S-DALINAC accelerator was calibrated in real time from readily-resolved reference transitions observed in the scattered radiation from Al and B wafers which sandwiched the In target. In order to cover an energy range $E_j \simeq 1.5$ - 4.5 MeV, measurements were performed at endpoints of 3.1, 4.6 and 5.2 MeV. The variation of E_0 also provided the means to distinguish ground-state (elastic) transitions from decays to excited states. Detailed scattering spectra are shown in the literature [59].

The integrated cross sections obtained from the excitation of the final state, ^{115}In^{m} and the photon scattering are shown in Fig. 12a. The excitation energies corresponding to the large $(\sigma\Gamma)_{fj}$ values of gateways are shown in the upper part of Fig. 12a. The widths of the histograms represent the experimental uncertainty in those energies. The striking result is that except for a few moderate levels around 3.0 and 3.7 MeV, all strongly scattering (γ,γ') transitions were found within the energy regions corresponding to the gateways. Thus, those transitions (or a

subset thereof) must have been responsible for the isomer population. No other (γ,γ') states were resolved in the lower part of Fig. 12a up to E_j = 5 MeV. This confirmed that all important pump bands in this range had been identified.

Further insight was attained from a theoretical analysis within the unified-model [58] which is well-suited to nuclei like ^{115}In near shell closure. The configuration space was built by proton 1h-states (relative to the semi-magic ^{116}Sn nucleus) and 1p-2h states across the major shell (relative to ^{114}Cd) coupled to collective phonons (up to three quadrupole and two octupole) in the underlying cores. A residual interaction was then used to mix the two subspaces. The comparison to experiment was accomplished by first computing all possible upward E1, M1, or E2 transitions in such a system. Then for states with a large partial width for transitions to the ground state, the full decay cascade was taken into account to determine model values for $(\sigma\Gamma)_{0j}$ and $(\sigma\Gamma)_{fj}$. In accordance with the experimental results, strong gateways were found only in a limited energy region above E_j = 2.5 MeV; typical $(\sigma\Gamma)_{fj}$ values at lower energies were reduced by a factor of about 10 - 100. The total number of important states was small, in agreement with the measurements.

Figure 12b presents the theoretical results which show a rough division of transition strengths into two groups which might be related to the experimental $(\sigma\Gamma)_{fj}$ data. Although a one-to-one correspondence seemed beyond the limits of the approach, simply summing the model $(\sigma\Gamma)_{fj}$ within each group compared favorably to the experimental values. The overall agreement seemed quite encouraging and indicated that no major part of the relevant configuration space was missed. A detailed analysis of the main decay branches revealed a clear picture of the important amplitudes in the gateway wavefunctions. All theoretical pump bands had $J^\pi = 7/2^+$ and the coupling to the ground state was dominated in all cases by single-particle $1g_{9/2} \rightarrow 1g_{7/2}$

spin-flip transitions. The first steps in the decays to the isomer in the model calculations proceeded mainly via E1 or E2 transitions.

The critical point to be made from this study, and supported by similar results [60] for the reaction $^{89}Y(\gamma,\gamma')^{89}Y^{m}$, is that nuclear structure theory, scattering measurements and photoactivation experiments all confirmed that giant pumping resonances corresponded to a small number of discrete gateways. Absorption cross sections approached those ideals of Eq. (6) needed to separate the wasted deposition of heat from the useful excitation of nuclei in a sample pumped with intense x rays.

I.3.2.4 Significance

The significance of these favorable developments to laser feasibility may be appreciated with the help of analogs from the atomic scale. In atoms there is a familiar increase in the density of levels available for excitation as transition energies approach the limit for photoionization. The number of such Rydberg states is generally on the order of n^3, where n is the principal quantum. Thus it is difficult to pump significant energy into a selected level with a continuum source of modest spectral width. The general difficulty in scaling x-ray lasers is a clear illustration of this problem and it seems that only the rigor imposed by selection rules allows the few cases demonstrated to work at all.

In nuclei the situation could have been even worse because the likelihood is much greater for there to be levels that from the atomic perspective would be considered analogous to multiply excited states. The nuclear level density is more difficult to specify quantitatively, but an approximation of exp ($\sqrt{n}$) is reasonably indicative as excitation energies approach that needed to remove the first particle in a photonuclear reaction. Since selection rules were shown to be bridged by the striking efficiency with which $\Delta K = 8$ could be lost in ^{180}Ta, there was a clear hazard that highly-excited nuclear levels could not be selectively excited as needed for a gamma-

ray laser. Sum rules limit the strength per unit bandwidth available at a particular transition energy and there was the possibility that the sum would be smoothly distributed over the great number of levels in any interval of high excitation. Then the deposition of pump energy into nuclear excitation would have been diluted into a much larger volume by the small cross sections available to any component transition. Such a distribution of gateway strength was not found, constituting a second breakthrough of comparable importance to that achieved by dumping the population of $^{180}Ta^{m}$.

The giant pumping resonances found in ^{115}In show the transition strength is concentrated into relatively few discrete lines. The nuclear structure model identified this particular case as an example of fragmented spin-flip transition strength, but the point critical to laser feasibility is the limited degree of the fragmentation. Relatively few transitions to gateway states collected all of that type of transition strength available over the range of energies from 2 - 5 MeV. The mechanism for this fragmentation was less clear, having arisen from detailed unified-model calculations.

An interesting speculation is currently being investigated [61,62] which may explain the existence of strong, low-multipolarity transitions similar to the giant pumping resonances in nuclei near mass 180. At certain energies of excitation, collective oscillations of the core nucleons may break the symmetry upon which rests the identification of angular-momentum projections of the pure single-particle states. Within this energy range single-particle states of differing K would be strongly mixed and the possibility for transferring larger amounts of ΔK with greater partial widths might be enhanced. Some support for this speculation has been found in unexpected enhancements to transitions which hinted at K mixing [61,62]. However, the most striking result was recently measured [63] for the spontaneous deexcitation of the 3.7-μs isomer $^{174}Hf^{m}$. There the decay of the isomer was found to occur primarily by a transition through a

state at 2685 keV in which sufficient K mixing occurred for $\Delta K = 14$ to be lost between the isomer and the ground-state bands. As shown in Fig. 13, this energy is remarkably close to that of the giant pumping resonance at 2800 ± 100 keV for ^{180}Ta, and other large gateways (Fig. 11) for neighboring nuclei in the mass-180 island. The energetics for giant pumping resonances for nuclei with quite dissimilar single-particle structures supports the identification of those gateways with K-mixing levels arising from a core property. In such a case, the integrated cross sections and excitation energies would be expected to vary slowly among neighboring nuclei. This behavior [56] is seen in Fig. 14 that plots the quantity S which is proportional to $(\sigma\Gamma)$ against nuclear deformation, a core property.

I.4 Thermal Economy of a Gamma-Ray Laser

Our final model of a gamma-ray laser is not fundamentally different from the nuclear analog of the ruby laser described [16] in 1982, envisioned as a thin film of diluent doped with isomeric nuclei and pumped with a flash of x rays in a slab geometry. The question of feasibility still rests on the degree to which the properties of some real nuclide approach those of the ideals being modeled. What has changed over the past half decade is that the discovery of giant pumping resonances has enabled some of the original constraints to be relaxed. The result is that the feasibility of a gamma-ray laser has been enhanced by orders-of-magnitude over that originally estimated in 1982. Thus, as summarized here it has been useful [57] to recompute the model in terms of the new data obtained during the past five years.

Since the better candidate isomers for a gamma-ray laser have never been fabricated in macroscopic amounts, precise knowledge of the properties of the best nuclide is not available. Moreover, since feasibility is such a complex function of the nuclear parameters, the

assumptions introduced into any model will critically affect the estimates of feasibility in strongly nonlinear ways. For the computation reported here the following parameters were assumed:

1) A single pump band exists which is a giant pumping resonance with a partial width of $b_a b_0 \Gamma = 1$ eV.

2) The pump transition is centered on an energy $E_i = 30$ keV.

3) The initial state is assumed to be isomeric with an excitation energy so high that 2) is possible.

4) The output transition is around 100 keV.

5) The active nuclei are diluted in a thin film of diamond or Be.

6) The Borrmann effect contributes a factor of 10 enhancement to the ratio of cross sections for resonant to nonresonant absorption.

The most sensitive assumptions are those of statements 2) and 3) about the width and excitation energy of the giant pumping resonance. The range of excitation energies over which isomers can be found is very large and it has already been shown experimentally that isomers can be dumped into freely-radiating states, even through $\Delta K = 8$ or $\Delta K = 14$. The only doubt here is a statistical one; whether or not a giant pump resonance can be found within 30 keV of an isomer.

Following our development [16] of 1982, under small signal conditions the midrange requirement of 10^{-4} is obtained for the pumped fraction,

$$\frac{N_f}{N_i} \geq \frac{\sigma_{NR}}{\sigma_R} \approx 10^{-4} \quad , \tag{9}$$

where σ_R and σ_{NR} are the cross sections for useful, resonant nuclear absorption and nonresonant photoelectric absorption, respectively. The value of 10^{-4} includes a Borrmann enhancement to

a value of $\sigma_{NR}/\sigma_R \approx 10^{-3}$ from Ref. [6]. Equation (9) sets the pump intensity needed for threshold, and with it the amount of waste heat to dissipate.

The essential concept in the management of the thermal economy is that the mean free path (MFP) for a photon resonant with the nuclear pump transition is much shorter than the MFP for nonresonant, photoelectric absorption to produce heat. Also, the MFP for a photoelectron produced in the nonresonant channel is greater in the diluent than the MFP for the photons pumping the nuclear resonance. This means that a thin film of diamond can be doped or implanted with active nuclei to provide useful absorption of incident photons in the bandwidth of the giant pumping resonance while the majority of the nonresonant photons will pass through the film into a substrate which can be cooled by ablation or cryogenics. Moreover, primary photoelectrons produced by the small fraction of nonresonant events occurring in the film can escape before their energy is degraded to heat.

The quantitative expression of this strategy is obtained by substituting Eq. (3) into Eq. (9) and assuming a single giant resonance dominates so that the sum is unnecessary. Solving for the spectral intensity, $\phi_j = \Phi_0 F(E_j,E_0)$ for 30 keV pump photons, the spectral fluence, $F_j \equiv E_j\phi_j$ at threshold is found to be

$$F_j = 177\ mJ\ cm^{-2}\ eV^{-1} \quad . \tag{10}$$

This gives the energy flux per unit bandwidth within the gateway resonance which must be incident upon the film.

For the likely cases of rare earth or platinide elements, the 30 keV pump energy lies below the K edge and about 15 keV above the L edge. As a result, primary photoelectrons produced by nonresonant absorption in the active medium should have energies on the order of

15 keV and ranges of 6.0 and 3.0 μm in Be and C, respectively [64]. Thus, only about 10% and 20% of the primaries, respectively, should be stopped in a 0.67 μm thick host film of Be or diamond. This thickness corresponds to the MFP for resonant absorption at a concentration of 10% doping. The fraction of the incident pump energy degraded into heat in the laser film because of nonresonant absorption becomes

$$f\,(Be) = 4.8 \times 10^{-4} \quad , \text{or} \tag{11a}$$

$$f\,(C) = 2.4 \times 10^{-4} \quad . \tag{11b}$$

Considering that edge filters or ablation layers could reduce the bandwidth of the pump radiation to 3 keV before reaching the doped layer of active medium, the incident fluence lying outside the bandwidth for resonant absorption would be 3000 times greater than the value of Eq. (10). However, only the fractions of Eqs. (11a) and (11b) are capable of being degraded into heat in the sensitive layer. The resulting energy balance can be summarized at threshold by the first two lines of Table IV.

Dividing those fluences by the 0.67 μm thickness gives the energy loading of the laser film shown in Table IV. These values are quite significantly below the levels of heating required to degrade the recoil-free fractions in the case of Be or diamond lattices. Baldwin has summarized [6] the involved dependence of the recoil-free fraction of gamma transitions upon recoil energy, lattice parameters, and temperature. He showed that even at a temperature, T equal to the Debye temperature, Θ_D, the recoil-free fraction is not significantly degraded (by more than a factor of 2) for a transition even so energetic as to give a classical recoil energy of 0.14 Θ_D. Since diamond is characterized by Θ_D = 2230 K, this means a transition of 100 keV is little affected by a temperature increase up to T = Θ_D. It is a textbook computation [65] to estimate that the energy content of the phonons for a material with Θ_D = 2230 K at a temperature of T = Θ_D is about 11 kJ cm^{-3}. Comparing this with the estimated thermal loading

of 3.8 kJ cm^{-3} gives a "safety factor" of almost three. A comparable margin is obtained for a Be lattice.

To summarize, it is convenient to recast the threshold fluence of Eq. (10) into more tangible terms. The spectral fluence of 177 mJ cm^{-2} eV^{-1} corresponds to 530 J cm^{-2} if the bandwidth of the pump x rays is arranged to be 3 keV, a practical separation which might be filtered between K edges. Even if pumped instantaneously so that no waste heat were transported away, the thermal loading would reach only 1/3 of the limit for retaining the Mössbauer effect in a diamond lattice. If derived from an x-ray line of 30 eV width, the threshold fluence would be only 5.3 J cm^{-2}. In that case the thermal loading would reach only 1/300 of the critical limit.

Even beyond this point much can be done to reduce heating further. All calculations so far considered the generation of the waste heat to be instantaneous. The time for the transit of a phonon across the 0.67-μm thickness of the inverting layer is on the order of only 100 ps so that the transport of significant amounts of heat into a diamond heat sink is possible on a nanosecond time scale. Yet most of the fluorescent levels of interest for inversion [16] have lifetimes of tens of nanoseconds to tens of microseconds. This is many times the period for the transport of phonons out of the film so that orders-of-magnitude can be realized in reducing the thermal loading further below the limits specified so far. However, all these techniques require precise knowledge about the energy levels and absorption edges of the materials involved. Until the properties of the best candidate for a gamma-ray laser are known, the exact specifications of the solution to the disposal of the waste heat cannot be generally articulated. The examples summarized here show that there are many orders-of-magnitude in the safety margin between likely amounts of heating and the much larger amounts which can be tolerated in stiff lattices such as Be and diamond.

I.5 Candidate Isomer for a Gamma-Ray Laser

I.5.1 Candidates and Simulations

An exact ranking of the 29 candidate isomers for a gamma-ray laser depends upon a complex weighting of combinations of nuclear parameters, many of which are poorly known. However, the potential importance of several nuclides is magnified by some very pragmatic considerations. These issues are typified by comparisons of the four examples presented in Table I.

From the perspective of shelf life and availability, $^{180}Ta^{m}$ is far superior. It is a naturally occurring material composing 0.012 % of all tantalum and can be prepared simply by separating natural Ta by atomic mass. Samples of milligram weight exist and one such specimen was used in the breakthrough experiment that proved x rays can dump the energy stored in isomeric populations. In contrast, the entire world inventory of $^{178}Hf^{m2}$ was reported in 1992 to be about 10^{15} nuclei [66] although recently this amount has been increased to about 5×10^{16}.

However, from the perspective of triggering $^{180}Ta^{m}$ appears to be much less practical. Although the energy storage is still impressively high, the isomeric level lies quite low in energy when compared to the value for the excitation of the K-breaking gateway at 2.8 MeV. For $^{178}Hf^{m2}$ the energy of the isomer at 2.45 MeV is the highest known that still lies below the likely gateway energy between 2.5 - 3.0 MeV [67]. The isomer $^{174}Hf^{m}$ is even higher at 3.312 MeV, but the availability [63] of a spontaneous transition down to the K-mixing level at 2.685 MeV reduces its shelf halflife to only 3.7 μs. Ideally for ease of triggering, an isomer would store as much energy as possible without exceeding that of the K-breaking level for that nuclide. As long as the transition energy needed for triggering is positive, the isomer cannot dump spontaneously as happens with $^{174}Hf^{m}$. The lifetime of the initial population will then be long

and problems of storage will be minimized. Guided to $^{178}Hf^{m2}$ by energetics, a reasonable next concern from the pragmatic viewpoint is for the duration of the trigger pulse.

Even in the best scenarios the requirement for the energy in a trigger pulse is large. The problem is compounded if the fluorescence lifetime of the level into which the isomeric population is to be dumped is too short. Large pulsed-power devices typically deliver their outputs over durations of nanoseconds to a few microseconds, so it would be desirable to utilize a laser candidate with strong fluorescence lines of comparable lifetimes. In this case as well, the $^{178}Hf^{m2}$ is favorable since it has transitions with lifetimes of both tens of ns and tens of μs, as will be seen in the following section.

The experiments needed to confirm our pragmatic scoring of the better of the 29 candidates for a gamma-ray laser have been postponed by the difficulties in obtaining samples. Thus, it has seemed fruitful to identify simulation nuclei which could serve as vehicles with which to develop systems and instrumentations for future triggering studies. To be useful a simulation nuclide needs to have a strong output fluorescence transition that can be reached by cascade from a K-breaking resonance pumped from the ground state by intense x-ray pulses. Moreover the levels radiating such transitions should have lifetimes of tens of ns to tens of μs. Meeting these criteria were the four convenient simulation nuclides listed in Table V whose excitation we have recently studied [68].

Excitation of those nuclides was provided by our 4 MeV Texas-X linac which produces 150-mA pulses of electrons of 4-μs duration at a repetition rate of 250 Hz. These are routinely converted to bremsstrahlung with a cooled Pt converter. The difficulty in this type of experiment which must be performed *in situ* lies in Compton scattering of the bremsstrahlung from the samples and a milligram-sized target support which produces background noise that tends to obscure gamma fluorescence. Our present system has used electronic gating to reduce

the sensitivity of the detector during the pump pulses. A combination of issues limits the recovery of the data acquisition system by a minimum product of fluorescence energy and delay time which currently is 150 keV x 2 μs. Shown in Fig. 15 are data [68] from delayed fluorescence at 482 keV from the 18-μs level of ^{181}Ta after a recovery time of 7.22 μs from the end of the x-ray pulse. The literature value of the fluorescence-state lifetime agrees well with the measured decay. The energetics of the process are summarized in the diagram of Fig. 16. Similar results are shown in Fig. 17 for the nuclide ^{176}Hf for which the relevant energy levels are summarized in Fig. 18. Analyses of the fluorescence data using Eqs. (1) - (4) yielded new values for the integrated cross sections for pumping of short-lived μs fluorescence. Figure 19 shows these results included in the summary plot of Fig. 11. It is encouraging to observe that the systematics for the pumping of these simulated laser levels closely follows the trends already established for the excitation of longer-lived levels which were easier to study. As yet the complementary data on the excitation energies needed to reach the pumping gateways have not been measured in these simulations, but they might reasonably be expected to also continue the established systematics.

I.5.2 First-Ranked Candidate

The first priority candidate for a gamma-ray laser is the 31-year isomer of ^{178}Hf, superior to the next possibilities by orders-of-magnitude. The energy-level diagram [69-71] for ^{178}Hf is shown in Fig. 20 with prominent fluorescent transitions indicated. The fundamental question is whether the giant pumping resonance will be found at the level shown in the figure that is predicted by systematics. In case of a weak success in which K-breaking is tending to fail we would expect pumping to preferentially populate the band to the right of the figure. This would lead to fluorescence at 437 keV with 35% efficiency from the bandhead having a 68-μs lifetime, well within current experimental capabilities demonstrated by the simulations.

In the event of a strong success in which K-breaking is complete, we would expect to preferentially populate the left-side band which leads to fluorescence at 922 keV with 65% efficiency and 1247 keV with 30% efficiency from the bandhead having a 78-ns lifetime. Demonstrations of dumping the stored energy from the isomer would then require the use of an accelerator with shorter pulses such as the APEX-I device in our facility. This e-beam machine produces 30 kA of electrons in pulses of 30-ns duration at energies variable from 0.7 - 1.2 MeV. Although a single-shot device, it served well in our first investigations of gamma fluorescence [36,42]. Moreover, there is a great advantage in the use of this type of device since it can be configured to use bremsstrahlung having 0.7 - 0.8 MeV endpoints to pump the left-side band that will give signal fluorescence at 1.25 MeV. It should be straightforward to set discrimination levels in the detection electronics to reject the scattered pump radiation which consists of photons at much lower energies.

The expected number of fluorescent photons can be calculated with two assumptions about the overall integrated cross section for pumping to fluorescence,

$$(\sigma\Gamma)_{sys} = 5 \times 10^{-25}\ cm^2\ keV \quad \text{, and} \tag{12a}$$

$$(\sigma\Gamma)_{best} = 2.5 \times 10^{-23}\ cm^2\ keV \quad , \tag{12b}$$

where the first value is consistent with the measurements of Fig. 19 and the second is scaled for the dependence on pump energy given by Eq. (6). The range of excitation energies spanned by the measurements of Figs. 11 and 19 is insufficient to determine any further correlation between ($\sigma\Gamma$) and the energy needed for triggering. For a target of 10^{15} nuclei, the Texas-X linac would produce 8×10^5 or 4×10^7 fluorescence photons per hour for the cross sections of Eqs. (12a) and (12b), respectively. In that case there is an ample safety margin for the arrangement of realistic geometries for the collection and detection of the fluorescence.

I.6 Conclusions

The current cycle of research into the feasibility of a gamma-ray laser started in 1982 with the emergence of a strongly interdisciplinary approach. Generally characterized by the study of nuclear analogs of concepts of quantum electronics already proven at the atomic and molecular levels, major advances have been realized in this period. Documented throughout this volume, they provide a richness of options for developing output coherence once excited nuclear states can be coupled to the radiation field.

Reviewed here have been our own works concerned with pumping (or triggering) enough nuclei into states which can be coupled when desired. Supported by strong collaborations with colleagues at the Technische Hochschule Darmstadt, the Flerov Laboratory for Nuclear Reactions at Dubna, and the CSNSM and IPN Laboratories at the Orsay Campus, major breakthroughs have been achieved that drastically improve the prospects for success. Primary has been the discovery of K-breaking levels in some nuclei at reasonably accessible energies. Unknown before 1988 [55], such levels have significance also in astrophysics [72], and were independently found in the decay of exotic nuclei [63] in 1990.

Transitions to the K-breaking levels provide giant pumping resonances which are analogous to the bandwidth funnels that made the ruby laser possible. Since they can be accessed either from ground states or from isomeric levels, K-breaking levels make *ex-situ* pumping of a gamma-ray laser a reasonable proposition. Precursive nuclides can be pumped into isomeric states either by reactors or by accelerators outside of the more fragile structures in which they would be used. Studies of systematics have shown the pervasive occurrence of K-breaking levels across islands of mass that contain the 29 candidate isomers originally preferred for a gamma-ray laser. In principle, many of these isomers could be produced *ex-situ* so that the requirements for triggering the conversion to freely-radiating states would represent

relatively modest demands for the remainder of the *in-situ* pumping to the K-breaking level. While computations of the thermal economy of the *in-situ* step depend upon high exponents of the unknown properties of the particular isomer and its host medium, reasonable targets are not necessarily destroyed by the waste pump power. Safety margins of orders-of-magnitude built into the estimates of thermal loading anticipate the emergence of parameter values less favorable than those modeled.

Most recently, an extension of the systematics studies has shown that the favorable occurrence of giant resonances for pumping nuclear fluorescence extends to the excitation of laser-like transitions having lifetimes on the order of μs. Also, the basic structural concept of doping the working nuclides into a thin diamond film at a target concentration of 10% has been demonstrated [73] and examples of Mössbauer nuclei implanted into diamond are already commercially available.

From the larger perspective it seems reasonable to conclude that the first breakthrough in determining the feasibility of a gamma-ray laser has been followed by a second. The proof that isomeric populations can be dumped by pumping them with intense pulses of x rays has been followed by the demonstration that the strengths for doing so are fragmented into relatively few discrete transitions of great intensity. These are precisely the necessary conditions for the concentration of useful pump power into the selective excitation of nuclear populations while dissipating power degraded to heat in much larger volumes. In the test case of ^{115}In, most amenable to computation, the pump step was found to be a spin-flip transition whose strength was only slightly fragmented into weaker components despite the higher state densities between 2 - 5 MeV. Complete agreement was demonstrated between our pumping measurements, independent scattering studies and theory in 1991 [59] and 1993 [74]. The particular structure of the K-breaking levels in the higher mass range of most importance has been proposed for the

case of ^{174}Hf [63]. We have tried to develop algorithms for rationalizing transition strengths in neighboring nuclides from scaling studies like that of Ref. [56], but the matter of accurate interpolation among the measurements remains a complex question.

While the paucity of actual samples has inhibited the final demonstration of feasibility, estimates of likely yields from such experiments have shown that strong levels of fluorescence from laser-like levels of the 31-year isomer ^{178}Hf^{m2} should be observable when the material becomes available. On the basis of shelflife and energy storage it seems a clear choice for the best candidate isomer for induced gamma-ray emission [67], a key triggering step in a gamma-ray laser. These conclusions would seem to provide a strong motivation for the production of this first ranked candidate for use in a gamma-ray laser.

The strongest conclusion to communicate here is that the persistent tenets of theoretical dogma which have historically [6] inhibited the development of a gamma-ray laser have been eliminated by experimental studies of the past five years. There is no need to melt the host lattice in order to pump a nuclear system to the laser threshold. There are no *a priori* obstacles to the realization of a gamma-ray laser. A gamma-ray laser seems feasible if the right combination of energy levels occurs in some real material. The overriding question to resolve is whether or not one of the better of the candidate nuclides has its isomeric level within a few tens or even hundreds of keV of one of the giant resonances for dumping angular momenta as seems to be the case with the priority candidate for a gamma-ray laser, ^{178}Hf^{m2}.

I.7 Continuing Organization

The end of the contracting period saw the crystallization of a community of interest in these interdisciplinary topics of induced gamma emission, IGE. A NATO ARW meeting gathered 46 research workers in this topic in 1995 to meet for critical review. On that occasion a standing commission, detailed as follows, was formed to encourage continued research.

ICIGE *International Commission on Induced Gamma Emission*

Exhibit I: Charter of Initial Organization

Advisory Board:

T. Arisawa	JAERI, Ibaraki JAPAN
C. B. Collins	Univ of Texas at Dallas, USA [ex. officio]
R. Coussement	Katholieke Univ Leuven, BELGIUM
G. R. Hoy	Old Dominion Univ, USA
Yu. Ts. Oganessian	JINR, Dubna, RUSSIA
L. A. Rivlin	MIREA, Moscow, RUSSIA
A. Sandulescu	Romanian Academy, ROMANIA
V. I. Zoran	IFIN, IFA, ROMANIA

Secretariat

Univ of Texas at Dallas
C. B. Collins, Dallas
Secretary General

National Technical Liasons US, Forrest J. Agee, Albuquerque

Administrative Centers

ICIGE Center at Bucharest
I. I. Popescu
Director
C. Ur
Scientific Secretary
E. Craciun
Secretary

Editorial Offices

J. J. Carroll, Youngstown
Editor
A. Zadernovsky, Moscow
Editor

I.8 References

1. Rivlin, L. A., *USSR Patent #621265*, Appl. January 10, 1961.
2. Baldwin, G. C., Neissel, J. P., Terhune, J. P., and Tonks, L., 1963, *Proc. IEEE*, **51**, 1247.
3. Vali, V. and Vali, W., 1963, *Proc. IEEE*, **51**, 182.
4. Rivlin, L. A., 1963, *Vopr. Radioelectron.*, **6**, 43.
5. Chirikov, B. V., 1963, *Sov. Phys. JETP*, **17**, 1355.
6. Baldwin, G. C., Solem, J. C., and Goldanskii, V. I., 1981, *Rev. Mod. Phys.* **53**, 678.
7. Letokhov, V. S., 1974, *Sov. J. Quant. Electron.*, **3**, 360.
8. Arad, B., Eliezer, S., and Paiss, Y., 1979, *Phys. Lett.* **74A**, 395.
9. Collins, C. B., Olariu, S., Petrascu, M., and Popescu, I., 1979, *Phys. Rev. Lett.*, **42**, 1397.
10. Collins, C. B., Olariu, S., Petrascu, M., and Popescu, I., 1979, *Phys. Rev. C*, **20**, 1942.
11. Olariu, S., Popescu, I., and Collins, C. B., 1981, *Phys. Rev. C*, **23**, 50.
12. Olariu, S., Popescu, I., and Collins, C. B., 1981, *Phys. Rev. C*, **23**, 1007.
13. Collins, C. B., in *Proceedings of the International Conference on Lasers '80*, ed. Collins, C. B., 1981 (STS Press, McLean, VA) p. 524-531.
14. Collins, C. B., in *Laser Technique for Extreme Ultraviolet Spectroscopy*, ed. McIlrath, T. J. and Freeman, R. R., 1982 (AIP Conf. Proc. No. 90, New York) p. 454-464.
15. Collins, C. B., in *Proceedings of the International Conference on Lasers '81*, ed. Collins, C. B., 1982 (STS Press, McLean, VA) p. 291-295.

16. Collins, C. B., Lee, F. W., Shemwell, D. M., DePaola, B. D., Olariu, S., and Popescu, I., 1982, *J. Appl. Phys.*, **53**, 4645.

17. DePaola, B. D. and Collins, C. B., 1984, *J. Opt. Soc. Am.*, **1**, 812.

18. Collins, C. B. and DePaola, B. D., in *Laser Techniques in the Extreme Ultraviolet*, eds. Harris, S. E., and Lucatorto, T. B., 1984 (AIP Conf. Proc. No. 119, New York) p. 45-53.

19. Collins, C. B. and DePaola B. D., 1985, *Optics Lett.*, **10**, 25.

20. DePaola, B. D., Wagal, S. S., and Collins, C. B., 1985, *J. Opt. Soc. Am. B*, **2**, 541.

21. DePaola, B. D. and Collins, C. B., 1984, *J. Opt. Soc. Am. B*, **1**, 812.

22. Collins, C. B., in *Handbook of Laser Science and Technology*, 1991 (CRC Press, Boca Raton) p. 561-567.

23. Pontecorvo, B. and Lazard, A., 1939, *C. R. Acad. Sci.*, *208, 99.*

24. Collins, G. B., Waldman, B., Stubblefield, E. M., and Goldhaber, M., 1939, *Phys. Rev.*, **55**, 507.

25. Metzger, F. R., 1959, *Prog. Nucl. Phys.*, **7**, 54.

26. von Neumann-Cosel, P., Richter, A., Carroll, J. J., and Collins, C. B., 1991, *Phys. Rev. C*, **44**, 554.

27. Breit, G., and Wigner, E., 1936, *Phys. Rev.*, **49**, 519.

28. Watanabe, Y. and Mukoyama, T., 1979, *Bull. Inst. Chem. Res., Kyoto Univ.*, **57**, 72,

29. Krcmar, M. Ljubicic, A., Pisk, K., Logan, B., and Vrtar, M., 1982, *Phys. Rev. C*, **25**, 2097.

30. Bikit, I., Slivka, J., Anicin, I. V., Marinkov, L., Ruydic, A., and Hamilton, W. D., 1987, *Phys. Rev. C*, **35**, 1943.

31. Nelson, W. R., Hirayama, H., and Rogers, D. W. O., 1985, *Stanford Linear Accelerator Center Report No. SLAC 265* (unpublished).

32. Halbleib, J. A., and Mehlhorn, T. A., 1984, *ITS: The Integrated TIGER Series of Coupled Electron/Photon Monte Carlo Transport Codes, Sandia National Laboratories Report SAND84-0573* (unpublished).

33. Mohan, R., Chui, C., and Lidofsky, L., 1985, *Med. Phys.*, **12**, 595.

34. *Evaluated Nuclear Structure Data File*, 1986 (Brookhaven National Laboratory, Upton, New York).

35. Browne, E. and Firestone, R. B., 1986, *Table of Radioactive Isotopes*, (Wiley, New York) p. 180.

36. Anderson, J. A. and Collins, C. B., 1987, *Rev. Sci. Instrum.*, **58**, 2157.

37. Carroll, J. J., and Collins, C. B., 1994, in *Proc. Int. Conf. Lasers and Appl. (LASERS '93)* p. 171-178.

38. Collins, C. B., Carroll, J. J., Sinor, T. W., Byrd, M. J., Richmond, D. G., Taylor, K. N., Huber, M., Huxel, N., von Neumann-Cosel, P., Richter, A., Spieler, C., and Ziegler, W., 1990, *Phys. Rev. C*, **42**, R1813.

39. Booth, E. C. and Brownson, 1967, *Nucl. Phys.* **A98**, 529.

40. Guth, E., 1941, *Phys. Rev.*, **59**, 325.

41. Paiss, Y., Eberhard, C. D., and Collins, C. B., 1987, *J. de Phys.*, **48**, 131.

42. Anderson, J. A. and Collins, C. B., 1988, *Rev. Sci. Instrum.* **59**, 414.

43. Anderson, J. A., Carroll, J. M., Taylor, K. N., Carroll, J. J., Byrd, M. J., Sinor, T. W., Collins, C. B., Agee, F. J., Davis, D., Huttlin, G. A., Kerris, K. G., Litz, M. S., Whittaker, D. A., Pereira, N. R., and Gorbics, S. G., 1989, *Nucl. Instrum. Meth.*, **B40/41**, 1189.

44. Anderson, J. A., Eberhard, C. D., Taylor, K. N., Carroll, J. M., Carroll, J. J., Byrd, M. J., and Collins, C. B., 1989, *IEEE Trans. Nucl. Sci.*, **36**, 241.

45. Collins, C. B. , Anderson, J. A., Paiss, Y., Eberhard, C. D., Peterson, R. J., and Hodge, W. L., 1988, *Phys. Rev. C*, **38**, 1852.

46. Anderson, J. A., Byrd, M. J., and Collins, C. B., 1988, *Phys. Rev. C*, **38**, 2833.

47. Carroll, J. J., Richmond, D. G., Sinor, T. W., Taylor, K. N., Hong, C., Standifird, J. D., and Collins, C. B., 1993, *Rev. Sci. Instrum.*, **64**, 2298.

48. von Neumann-Cosel, P., Huxel, N., Richter, A., Spieler, C., Carroll, J. J., and Collins, C., B., 1994, *Nucl. Instrum. Meth.*, **A338**, 425.

49. Carroll, J. J., Byrd, M. J., Richmond, D. G., Sinor, T. W., Taylor, K. N., Hodge, W. L., Paiss, Y., Eberhard, C. D., Anderson, J. A., Collins, C. B., Scarbrough, E. C., Antich, P. P., Agee, F. J., Davis, D., Huttlin, G. A., Kerris, K. G., Litz, M. S., and Whittaker, D. A., 1991, *Phys. Rev. C*, **43**, 1238.

50. *Nuclear Theory, Vol. 2: Excitation Mechanisms of the Nucleus, Electromagnetic and Weak Interactions*, Eisenberg, J. M., and Greiner, W., 1970 (North Holland, Amsterdam) Parts I and II.

51. Carroll, J. J., Sinor, T. W., Richmond, D. G., Taylor, K. N., Collins, C. B., Huber, M. Huxel, N., von Neumann-Cosel, P., Richter, A., Spieler, C., and Ziegler, W., 1991, *Phys. Rev. C*, **43**, 879.

52. *ASTM Standard Method for Determining Thermal Neutron Reaction and Fluence Rates by Radioactivation Techniques, Publication E 262-86*, 1987 (American Society for Testing and Materials, Philadelphia) and references cited there.

53. Anderson, J. A., Eberhard, C. D., Carroll, J. J., Byrd, M. J., and Collins, C. B., in *Center for Quantum Electronics Annual Report FY-1988*, 1988 (unpublished) p.147-176.

54. *ASTM Standard Method for Determining Neutron Flux, Fluence, and Spectra by Radioactivation Techniques, Publication E 261-77*, 1987 (American Society for Testing and Materials, Philadelphia) and references cited there.

55. Collins, C. B., Eberhard, C. D., Glesener, J. W., and Anderson, J. A., 1988, *Phys. Rev. C*, **37**, 2267.

56. Collins, C. B., Carroll, J. J., Taylor, K. N., Richmond, D. G., Sinor, T. W., Huber, M., von Neumann-Cosel, P., Richter, A., and Ziegler, W., 1992, *Phys. Rev. C*, **46**, 952.

57. Collins, C. B., Carroll, J. J., Taylor, K. N., Sinor, T. W., Hong, C., Standifird, J. D., and Richmond, D. G., 1992, *Laser Interaction and Related Plasma Phenomenon*, eds. Miley, G. H., and Hora, H. (Plenum, NY) **10**, 151.

58. Ziegler, W., Rangacharyulu, C., Richter, A., and Spieler, C., 1990, *Phys. Rev. Lett.*, **65**, 2515.

59. von Neumann-Cosel, P., Richter, A., Spieler, C., Ziegler, W., Carroll, J. J., Sinor, T. W., Richmond, D. G., Taylor, K. N., Collins, C. B., and Heyde, K., 1991, *Phys. Lett. B*, **266**, 9.

60. Huber, M., von Neumann-Cosel, P., Richter, A., Schlegel, C., Schulz, R., Carroll, J. J., Taylor, K. N., Richmond, D. G., Sinor, T. W., Collins, C. B., and Ponomarev, V., Yu., 1993, *Nucl. Phys.*, **A559**, 253.

61. Friedrichs, H., Lindenstruth, S., Schlitt, B., Wesselborg, C., Bauske, I., Heil, R. D., Kneissl, U., Margraf, J., Pitz, H. H., Häger, D., Müller, G., Schumacher, M., von Brentano, P., Herzberg, R. D., and Zilges, A., 1993, *Nucl. Phys.*, **A553**, 553.

62. Xie, H., Ender, Ch., Gerl, J., Härtlein, Th., Köck, F., Kröll, Th., Reiter, P., Schwalm, D., Thirolf, P., Vetter, K., Wieswesser, A., and Wollersheim, H. J., 1993, *Phys. Rev. C*, **48**, 2517.

63. Walker, P. M., Sletten, F., Gjørup, N. L., Bentley, M. A., Borggreen, J., Fabricius, B., Holm, A., Howe, D., Pedersen, J., Roberts, J. W., and Sharpey-Schafer, J. F., 1990, *Phys. Rev. Lett.*, **65**, 416.

64. Knopf, G., and Paul, W., in *Alpha, Beta and Gamma-Ray Spectroscopy*, ed. Siegbahn, K., 1965 (North Holland, Amsterdam) p. 1 - 25.

65. *Introduction to Solid State Physics, 6th Edition*, Kittel, C., 1986 (Wiley, New York) p. 106.

66. Oganessian, Yu. Ts., Karamian, S. A., Gangrski, Y. P., Gorski, B., Markov, B. N., Szeglowski, Z., Briançon, Ch., Ledu, D., Meunier, R., Hussonnois, M., Constantinescu, O., and Subbotin, M. I., 1992, *J. Phys. G: Nucl. Part. Phys.*, **18**, 393.

67. Collins, C. B., Carroll, J. J., Oganessian, Yu. Ts., and Karamian, S. A., 1995, *Laser Physics*, **5**, 209.

68. Hong, C., Taylor, K. N., Carroll, J. J., Sinor, T. W., and Collins, C. B. (in preparation).

69. Khoo, T. L., and Løvhøiden, G., 1977, *Phys. Lett.*, **67B**, 271.

70. Sheline, R. K., Burke, D. G., Minor, M. M., and Sood, P. C., 1993, *Phys. Rev. C*, **48**, 911.

71. *National Nuclear Data Center Online Evaluated Nuclear Structure Data File (ENSDF)*, 1994, Brookhaven National Laboratory.

72. Carroll, J. J., Anderson, J. A., Glesener, J. W., Eberhard, C. D., and Collins, C. B., 1989, *Astrop. J.*, **344**, 454.

73. Sinor, T. W., Standifird, J. D., Davanloo, F., Taylor, K. N., Hong, C., Carroll, J. J., and Collins, C. B., 1994, *Appl. Phys. Lett.*, **64**, 1221.

74. Carroll, J. J., Collins, C. B., Heyde, K., Huber, M., von Neumann-Cosel, P., Ponomarev, V. Yu., Richmond, D. G., Richter, A., Schlegel, C., Sinor, T. W., and Taylor, K. N., 1993, *Phys. Rev. C*, **48**, 2238.

TABLE I

Summary of important properties [35] of four of the 29 most promising candidate isomers for a gamma-ray laser.

Isomer	Energy Density [J/μg]	Shelf Halflife, $T_{1/2}$	Trigger Photon [MeV]
$^{177}Hf^{m}$	1,500	51 min	~ 0
$^{178}Hf^{m2}$	1,300	31 yr	< 0.5
$^{179}Hf^{m}$	600	25 d	~ 1.5
$^{180}Ta^{m}$	40	> 10^{15} yr	~ 2.8

TABLE II

Summary of nuclides, and excitation energies, E_j and integrated cross sections for their gateway states, that are sufficiently well-known from the literature to permit their use as calibration standards. Some integrated cross sections were calculated by Eqs. (5) and (6) using constituent parameters found in the literature [34,35], while other values were directly obtained in the referenced experiments.

Isomer	$T_{1/2}$	E_{fluor} [keV]	E_j [MeV]	$(\sigma\Gamma)_{0j}$ [10^{-29} cm^2 keV]
Levels useful below 1.4 MeV [36,39,42]				
$^{77}Se^m$	17.45 s	162	0.250	0.20
			0.480	0.87
			0.818	0.7
			1.005	30
$^{79}Br^m$	4.9 s	207	0.761	5.9
$^{87}Sr^m$	2.8 h	388	1.2	8.5
$^{115}In^m$	4.5 h	336	1.078	18.7
Levels useful below 4 MeV [39,47,48,75]				
$^{79}Br^m$	4.9 s	207	1.8	65
$^{87}Sr^m$	2.8 h	388	1.9	16
			2.7	430
$^{115}In^m$	4.5 h	336	1.4	64
			1.6	10.1
			2.8	540
			3.3	760
$^{137}Ba^m$	2.6 min	662	3.2	220

TABLE III

Recently measured values [38] of integrated cross sections and excitation energies for gateways in the reaction $^{180}Ta^{m}(\gamma,\gamma')^{180}Ta$.

E_j [MeV]	$(\sigma\Gamma)_{fj}$ [10^{-29} cm^2 keV]
2.8 $\pm$ 0.1	12,000 $\pm$ 2,000
3.6 $\pm$ 0.1	35,000 $\pm$ 5,000

TABLE IV

Summary of the thermal economy at threshold for a gamma-ray laser nuclide doped into a film of 0.67-μm thickness of the low-Z materials shown.

Quantity	Material	
	Be	C (Diamond)
Resonant input fluence	177 mJ cm^{-2}	177 mJ cm^{-2}
Fluence degraded to heat	127 mJ cm^{-2}	255 mJ cm^{-2}
Resonant energy density	2.6 kJ cm^{-3}	2.6 kJ cm^{-3}
Thermal loading	1.9 kJ cm^{-3}	3.8 kJ cm^{-3}

TABLE V

Summary of properties [35,71] of nuclides useful in simulating the pumping of the better of the 29 candidates for a gamma-ray laser.

Nuclide	Abundance [%]	Output transitions [keV]	Fluorescence lifetime [μs]
^{81}Br	49.31	260 276	37.6
^{176}Hf	5.206	736 1043	9.6, 9.9
^{181}Ta	99.998	346 482	18
^{201}Hg	13.1	521	92

CAPTIONS

Figure 1: Schematic representation of the pumping of a fluorescence level through a pump band, or gateway state, of natural width Γ. The initial level from which population is excited with an absorption cross section σ_0 can be either a ground state or an isomer. The branching ratios b_a and b_o give the probabilities that the gateway will decay directly back to the initial state, and directly or by cascade to the fluorescence level, respectively. Only a single gateway is shown but there could be more; the index j is used to identify individual pump bands.

Figure 2: (a) Calculated spectral distribution function, $F(E,E_0)$ for a typical bremsstrahlung continuum (dashed line) with an endpoint of E_0 = 3.5 MeV plotted with the left-hand axis. Gateway excitation energies and integrated cross sections available from the earlier literature [39] are shown by the thin vertical bars and are plotted with the right-hand axis. The thick vertical bar indicates a gateway found in the recent experiments of Ref. [38]. All gateway parameters are listed in Table II. (b) Measured activations, $A_f(E_0)$ obtained using five different accelerators [37,38,49] for the reaction $^{87}Sr(\gamma,\gamma')^{87}Sr^m$ plotted with symbols as functions of bremsstrahlung endpoint. The solid curve plots the expected excitation function computed with the model of Eqs. (1) - (6).

Figure 3: Spectral intensity expressed in units of total photon energy per unit bandwidth for 1.4-MeV bremsstrahlung from DNA/PITHON measured [42] using the XAN technique (symbols) with the gateway parameters of Table II, compared with a spectrum computed (curve) with the TIGER code [32]. Uncertainties of the measured points are comparable to the size of the symbols except where otherwise indicated.

Figure 4: Instantaneous spectral intensity, ϕ for 4-MeV bremsstrahlung from the Texas-X measured [47] using the XAN technique (symbols) with the gateway parameters of Table II, compared with a spectrum computed (lines) with the EGS4 code [31]. Statistical errors associated with the calculations are indicated by the bars on the histograms. Uncertainties of the measured points are comparable to the size of the symbols except where otherwise indicated.

Figure 5: Fluorescence data [49] from the decay of $^{167}Er^{m}$ following its excitation with 6-MeV bremsstrahlung from a medical linac for an irradiation of 25 s. The pulse-height (energy) spectrum of (a) and the multichannel-scalar (decay) spectrum of (b) were obtained using a NaI(Tl) spectrometer. The measurements of fluorescence energy and lifetime were in excellent agreement with the literature values [35].

Figure 6: Fluorescence data [49] from the decay of $^{123}Te^{m}$ following its excitation with 6-MeV bremsstrahlung from a medical linac for an irradiation of 2 h. The pulse-height (energy) spectrum of (a) and the counting-rate (decay) spectrum of (b) were obtained using a HPGe spectrometer. Counting periods used to obtain the measurements of (b) were 10 h. The measurements of fluorescence energy and lifetime were in excellent agreement with the literature values [35].

Figure 7: Schematic energy-level diagram [34,55] of ^{180}Ta and its daughters. Energies are given in keV and the halflives of the tantalum ground state and the isomer are shown. The upward arrow indicates the pump transition to the gateway represented by the hatched level. The cascade from the gateway is unknown but leads to the ground state which transmutes to the

two daughters by electron capture and beta decay. The primary signatures of the decay of the ground state are K lines from ^{180}Hf characterized by the lifetime of the parent, ^{180}Ta^{g}.

Figure 8: Pulse-height spectra [55] showing fluorescence counting rates from an enriched sample of ^{180}Ta^{m} before (dotted) and after (solid) irradiation with the 6-MeV medical linac. The measurements were made with a HPGe spectrometer. The prominent K lines from daughter ^{180}Hf nuclei produced by decay of ^{180}Ta ground states indicate the dumping of significant numbers of ^{180}Ta isomers in this mg-sized sample.

Figure 9: Decay spectrum [55] plotting counting rates measured for the Hf K_{α} lines seen in Fig. 8 as a function of time elapsed from the end of the irradiation. The measurements were made over the intervals shown and uncertainties in the observations were comparable to the size of the plotted symbols. The measured decay rate was in excellent agreement with the literature value [35].

Figure 10: (a) Calculated spectral distribution function, $F(E,E_0)$ for a typical bremsstrahlung continuum (dashed line) with an endpoint of $E_0 = 3.5$ MeV plotted with the left-hand axis. Gateway excitation energies and integrated cross sections measured in the experiments of Ref. [38] are shown by the thick vertical bars and are plotted with the right-hand axis. (b) Measured activations, $A_f(E_0)$ obtained with the S-DALINAC [38] for the reaction ^{180}Ta$^{m}(\gamma,\gamma')^{180}$Ta plotted with symbols as functions of bremsstrahlung endpoint. The activation edge at 2.8 ± 0.1 MeV indicated the excitation energy of the lowest gateway; its magnitude was sufficient to characterize it as a giant pumping resonance.

Figure 11: Integrated cross sections and excitation energies, plotted with the left-hand and right-hand axes, respectively, for gateways measured in the experiments of Refs. [38,49,56] which pump or dump populations of isomers. The groupings of pumping strengths seen in the figure correspond to mass islands between magic numbers for neutrons and protons. The best candidates for a gamma-ray laser lie within the mass-180 island which contains the largest values of integrated cross section corresponding to giant pumping resonances. Within each island, the integrated cross sections and gateway excitation energies vary only slowly with changing mass number, A, despite differing single-particle structures among neighboring nuclides.

Figure 12: Comparison of integrated cross sections [59] for ^{115}In plotted as functions of gateway excitation energy, E_j, obtained from (a) experimental measurements and (b) unified-model calculations. The upper panels show values of $(\sigma\Gamma)_{fj}$ of Eq. (5) for the photoexcitation reaction $^{115}In(\gamma,\gamma')^{115}In^m$, while the lower panels show values of $(\sigma\Gamma)_{0j}$ of Eq. (8) for elastic photon scattering, $^{115}In(\gamma,\gamma)^{115}In$.

Figure 13: Energetics for the spontaneous decay of the 3.7-μs isomer $^{174}Hf^m$ through a K-mixing level at 2.6 MeV which provided $\Delta K = 14$, compared with that for the dumping of populations of $^{180}Ta^m$ through a giant pumping resonance at 2.8 ± 0.1 MeV which provided $\Delta K = 8$. Both intermediate levels are expected to be admixtures of single-particle states having differing values of the K quantum number.

Figure 14: Isomer excitation probabilities, S plotted as a function of ground-state deformation, δ showing a slow variation consistent with a core property for the giant pumping resonances [56]. The quantity $S \equiv (\sigma\Gamma)_{fj}/E_j$, defined assuming a dipole character for the absorption step,

is summed over the energy region 2 - 4.5 MeV and is proportional to the reduced transition probability.

Figure 15: Fluorescence detected at 482 keV from the decay of the 615 keV isomer of ^{181}Ta. The data were obtained [68] using a gated detector system and corresponded to nearly 10^6 acquisition cycles taken over 45 min. The solid line shows a fit to the data which agrees well with the literature value [34] for the lifetime of the 615-keV level.

Figure 16: Schematic diagram showing the energy levels [71] important for the excitation of the 615-keV, 18-μs state in ^{181}Ta. The large upward arrow indicates the absorption transition to a gateway located [68] near 2.8 MeV which populates that laser-like level by a branch of its decay cascade (shown by the dashed arrow). Transitions providing photons used to detect the fluorescence are indicated with their energies.

Figure 17: Fluorescence detected from the decay of the 1333 keV isomer of ^{176}Hf. The data were obtained [68] using a gated detector system and corresponded to nearly 10^5 acquisition cycles taken over 5 min. The solid line shows a fit to the data which agrees well with the literature value [34] for the lifetime of the 1333-keV level.

Figure 18: Schematic diagram showing the energy levels [71] important for the excitation of the 1333-keV, 9.6-μs state in ^{176}Hf. The large upward arrow indicates the absorption transition to a gateway located [68] near 2.8 MeV which populates that laser-like level by a branch of its decay cascade (shown by the dashed arrow). Transitions providing photons used to detect the fluorescence are indicated with their energies.

Figure 19: Integrated cross sections for populating laser-like levels in the simulation nuclei superimposed on those of Fig. 11 for the pumping and dumping of long-lived isomers. Again, the groupings correspond to mass islands between magic numbers and the best candidates are identified as neighbors of ^{180}Ta.

Figure 20: Schematic energy-level diagram [69-71] of ^{178}Hf. The spontaneous decay of the 31-year isomer proceeds through an yrast band which does not excite transitions in the left-hand K = 6 band or the K = 14 band. The 68-μs bandhead decays by cascade through the right-hand K = 8 band. The position of the K-mixing giant pumping resonance inferred from systematics is shown by the wide shaded band near 2.8 MeV and the large upward arrow indicates the pump transition from the 31-year isomer. Transitions providing fluorescence photons useful for the detection of the pumping reaction are identified along with their energies.

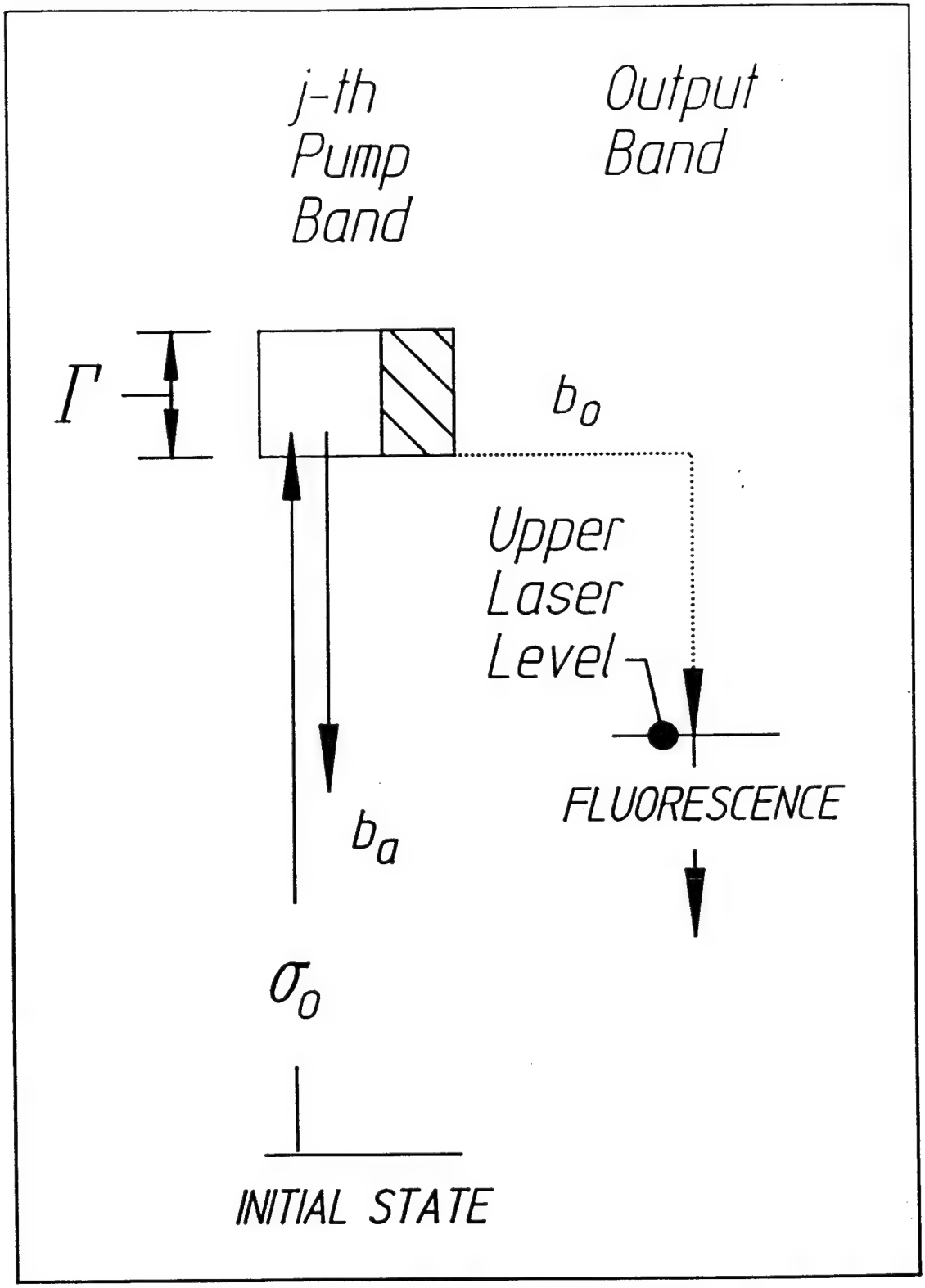
j-th
Pump
Band
Output
Band
Γ
b_o
Upper
Laser
Level
FLUORESCENCE
b_a
σ_o
INITIAL STATE

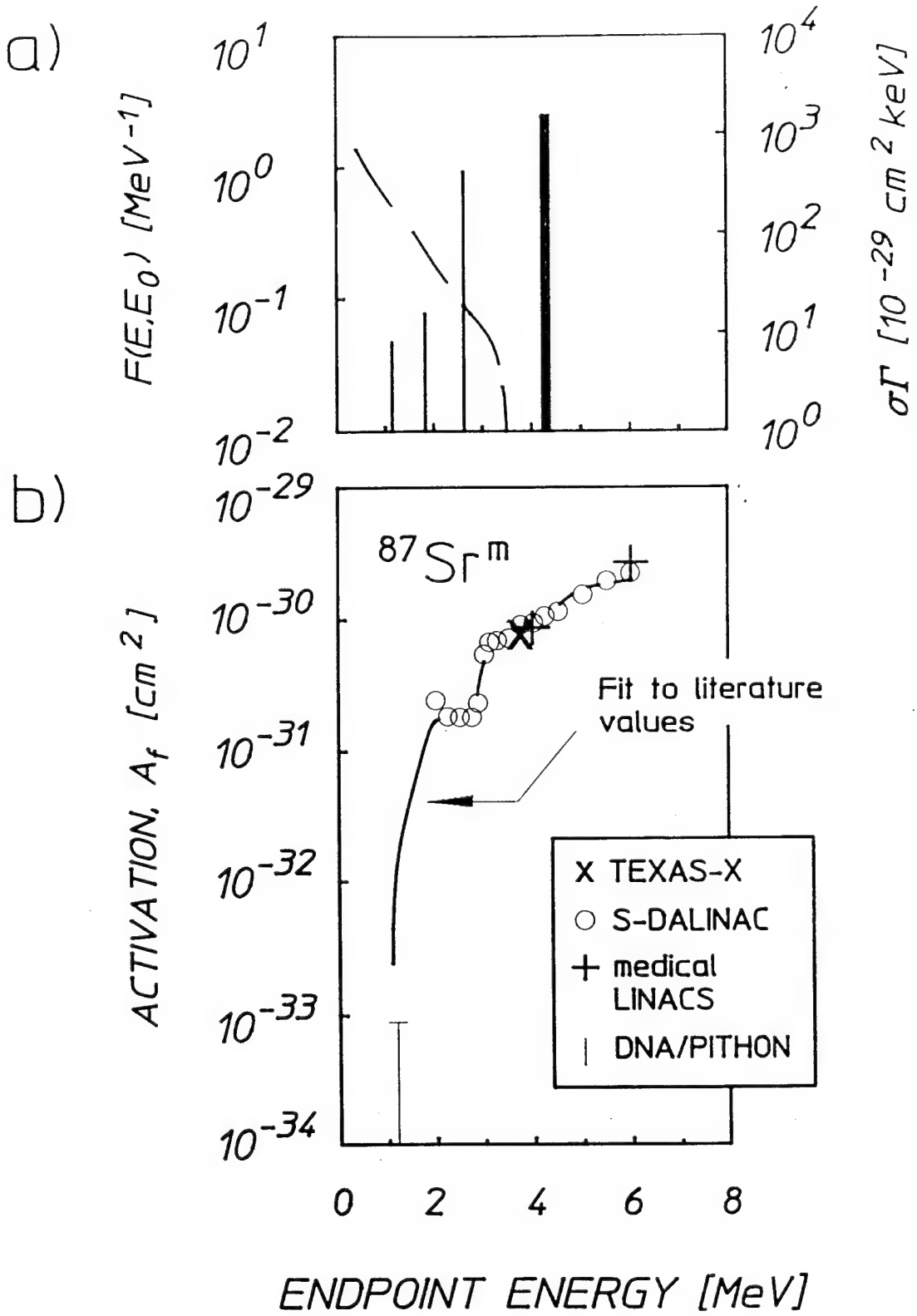
a)
b)
10^{1}
10^{0}
10^{-1}
10^{-2}
$F(E,E_0)$ [MeV^{-1}]
10^{4}
10^{3}
10^{2}
10^{1}
10^{0}
$\sigma\Gamma$ [10^{-29} cm^2 keV]
10^{-29}
10^{-30}
10^{-31}
10^{-32}
10^{-33}
10^{-34}
ACTIVATION, A_f [cm^2]
$^{87}Sr^{m}$
Fit to literature values
X TEXAS-X
○ S-DALINAC
+ medical LINACS
| DNA/PITHON
0
2
4
6
8
ENDPOINT ENERGY [MeV]

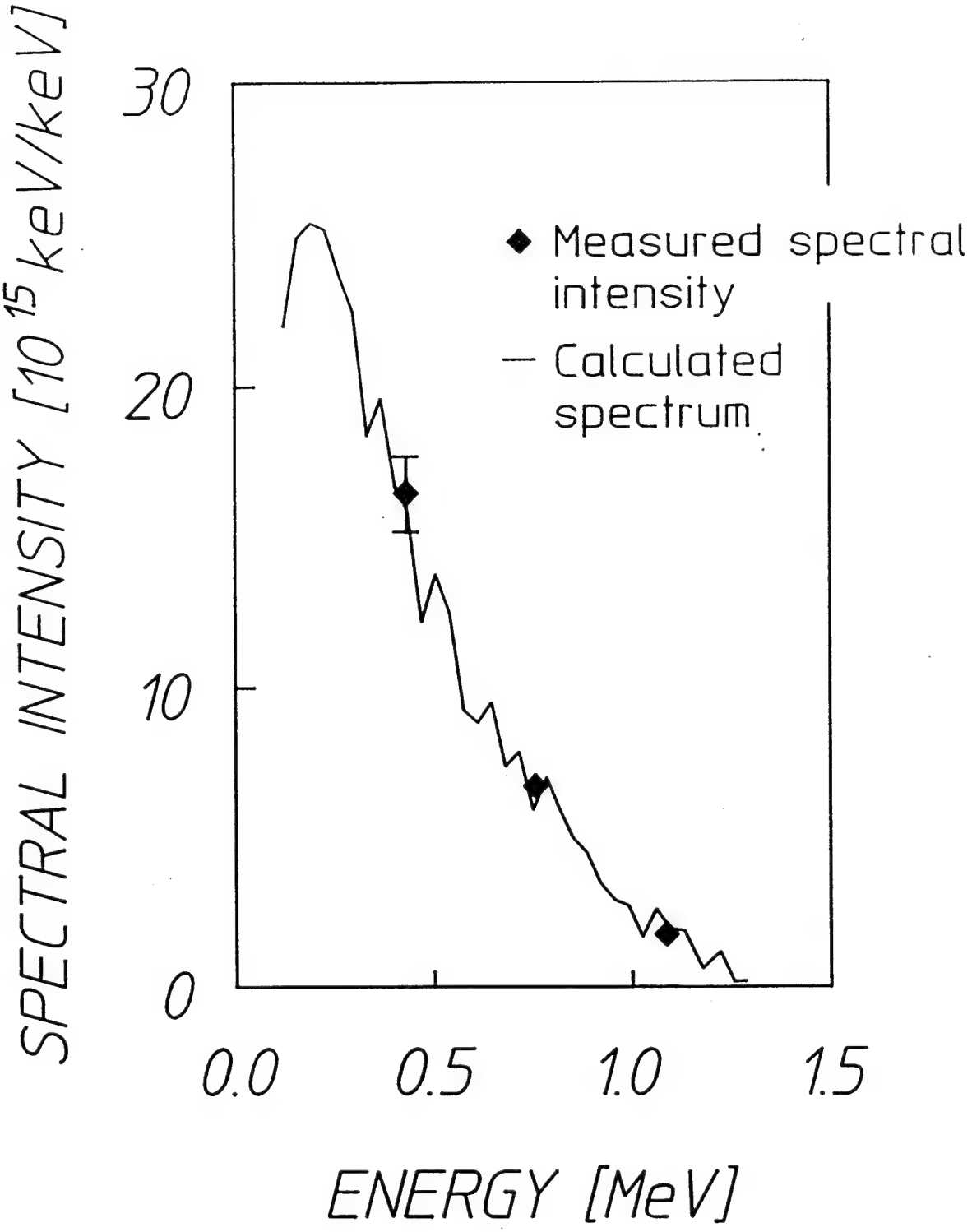
SPECTRAL INTENSITY [10^15 keV/keV]
30
20
10
0
0.0
0.5
1.0
1.5
ENERGY [MeV]
Measured spectral intensity
Calculated spectrum

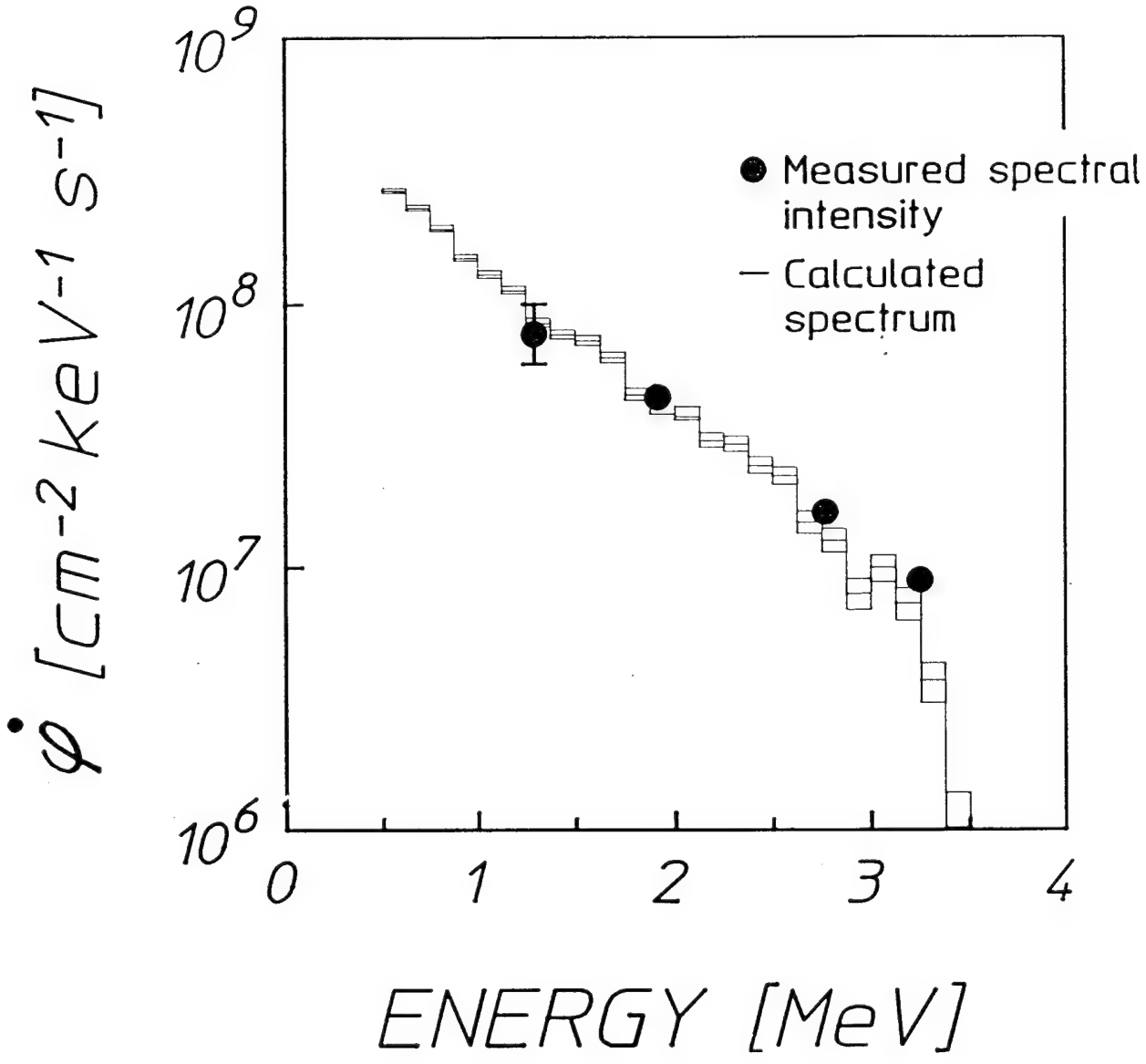
10^9
10^8
10^7
10^6
$\dot{\varphi}$ [cm^{-2} keV^{-1} s^{-1}]
Measured spectral intensity
Calculated spectrum
0
1
2
3
4
ENERGY [MeV]

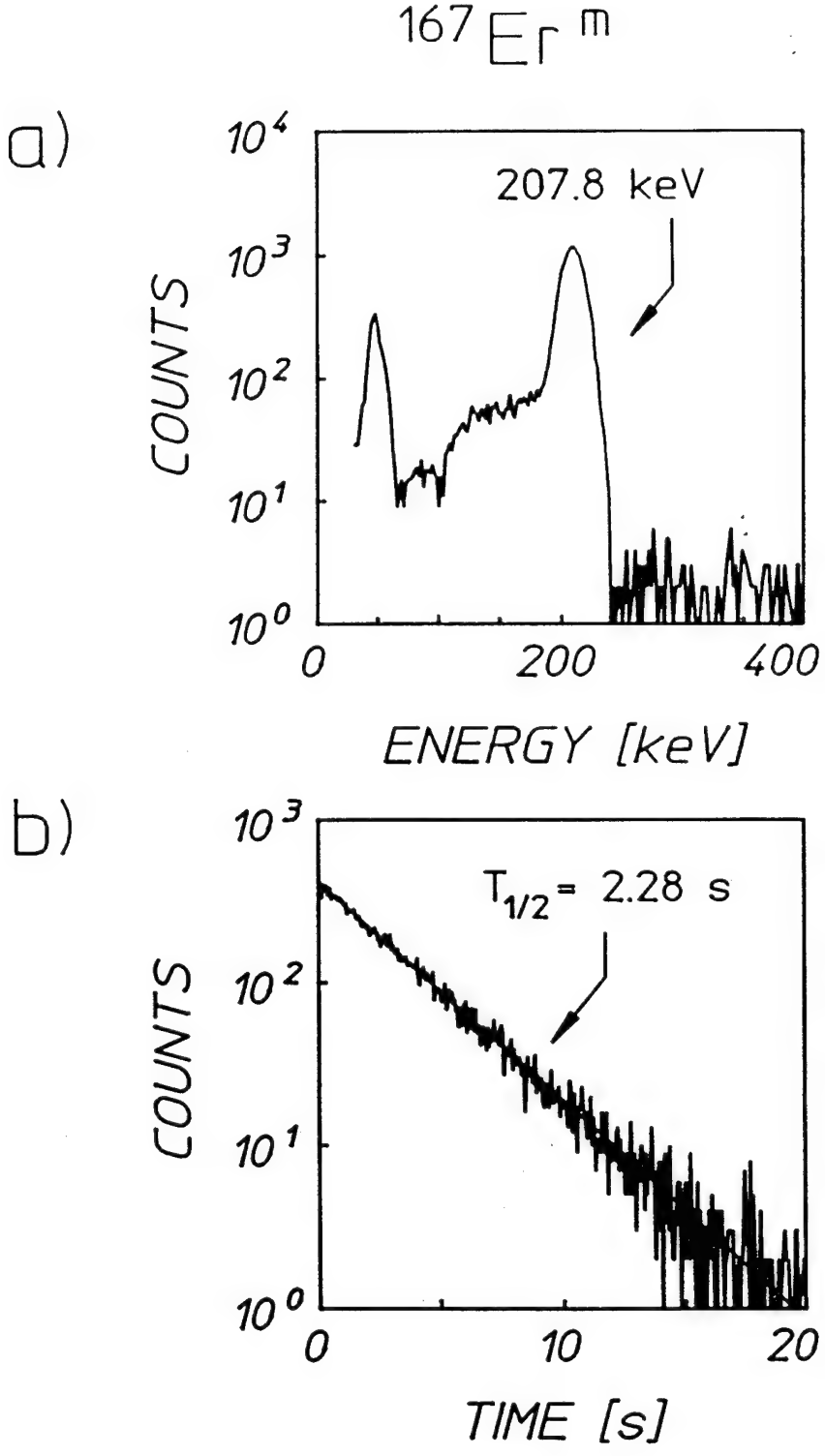
167 Er m
a)
10^4
10^3
10^2
10^1
10^0
COUNTS
207.8 keV
0
200
400
ENERGY [keV]
b)
10^3
10^2
10^1
10^0
COUNTS
T1/2 = 2.28 s
0
10
20
TIME [s]

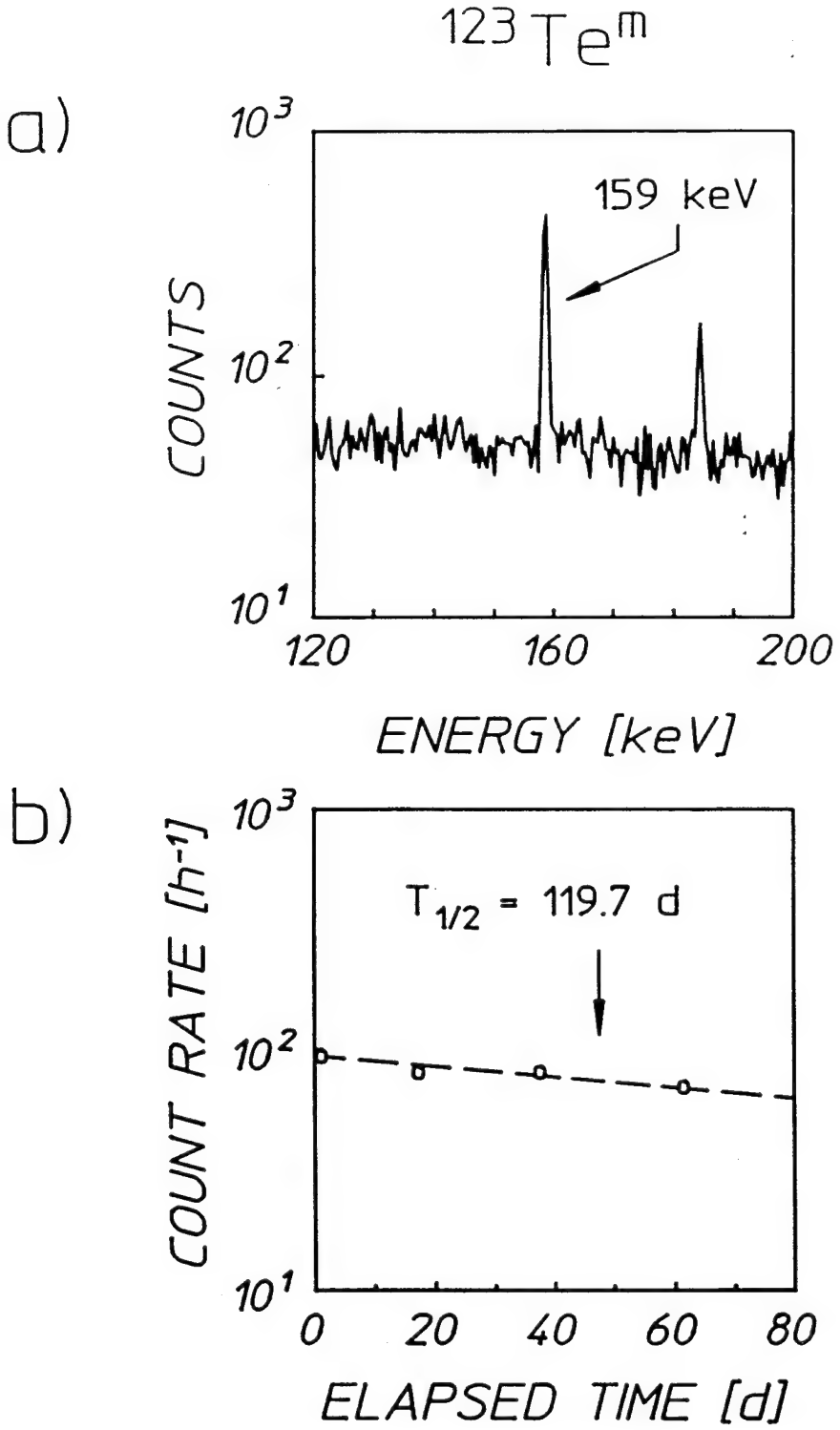
123 Te m
a)
10 3
10 2
10 1
COUNTS
159 keV
120
160
200
ENERGY [keV]
b)
10 3
10 2
10 1
COUNT RATE [h-1]
T 1/2 = 119.7 d
0
20
40
60
80
ELAPSED TIME [d]

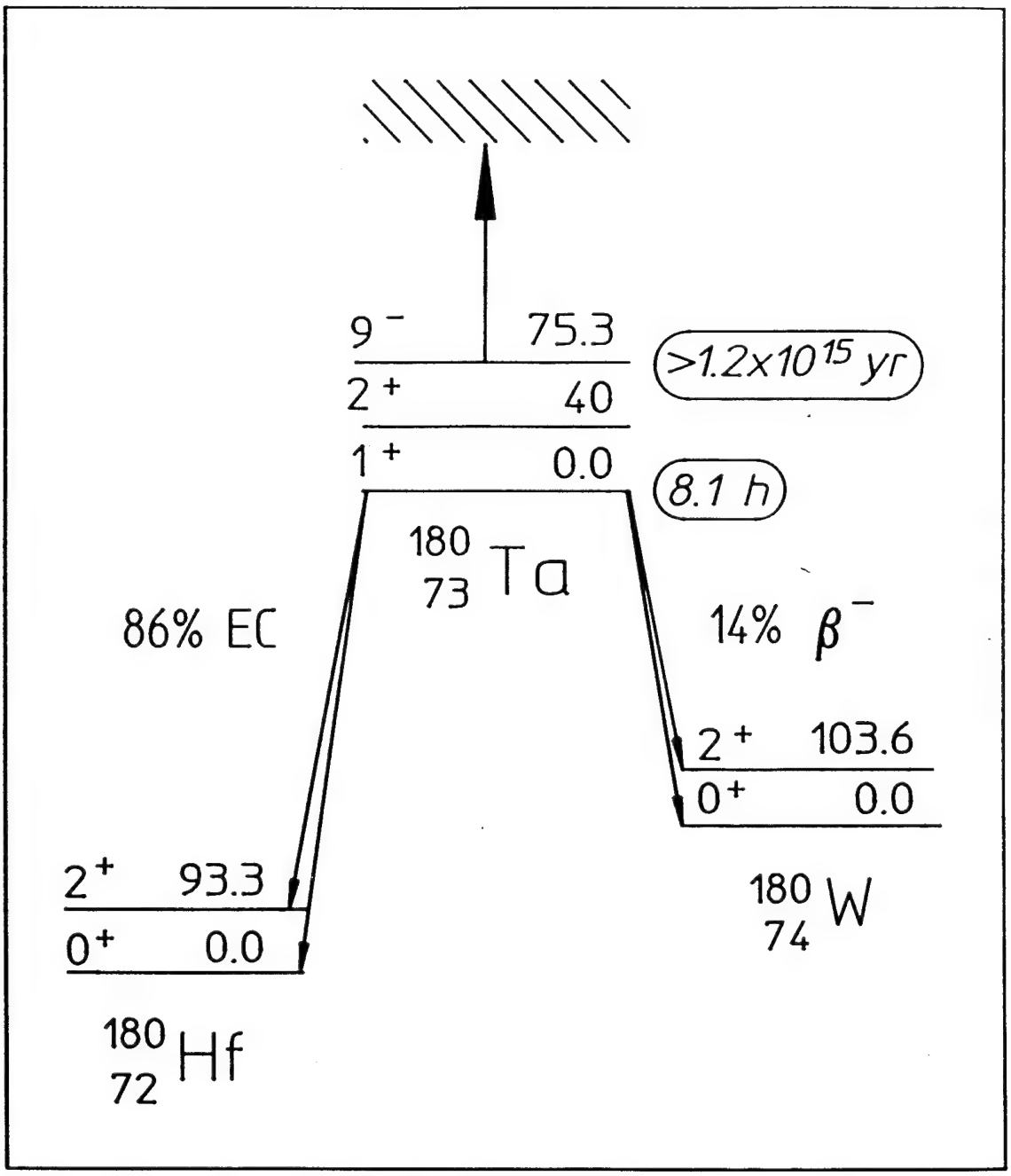
9⁻ 75.3
2⁺ 40
1⁺ 0.0
>1.2x10¹⁵ yr
8.1 h
180 73 Ta
86% EC
14% β⁻
2⁺ 103.6
0⁺ 0.0
2⁺ 93.3
0⁺ 0.0
180 74 W
180 72 Hf

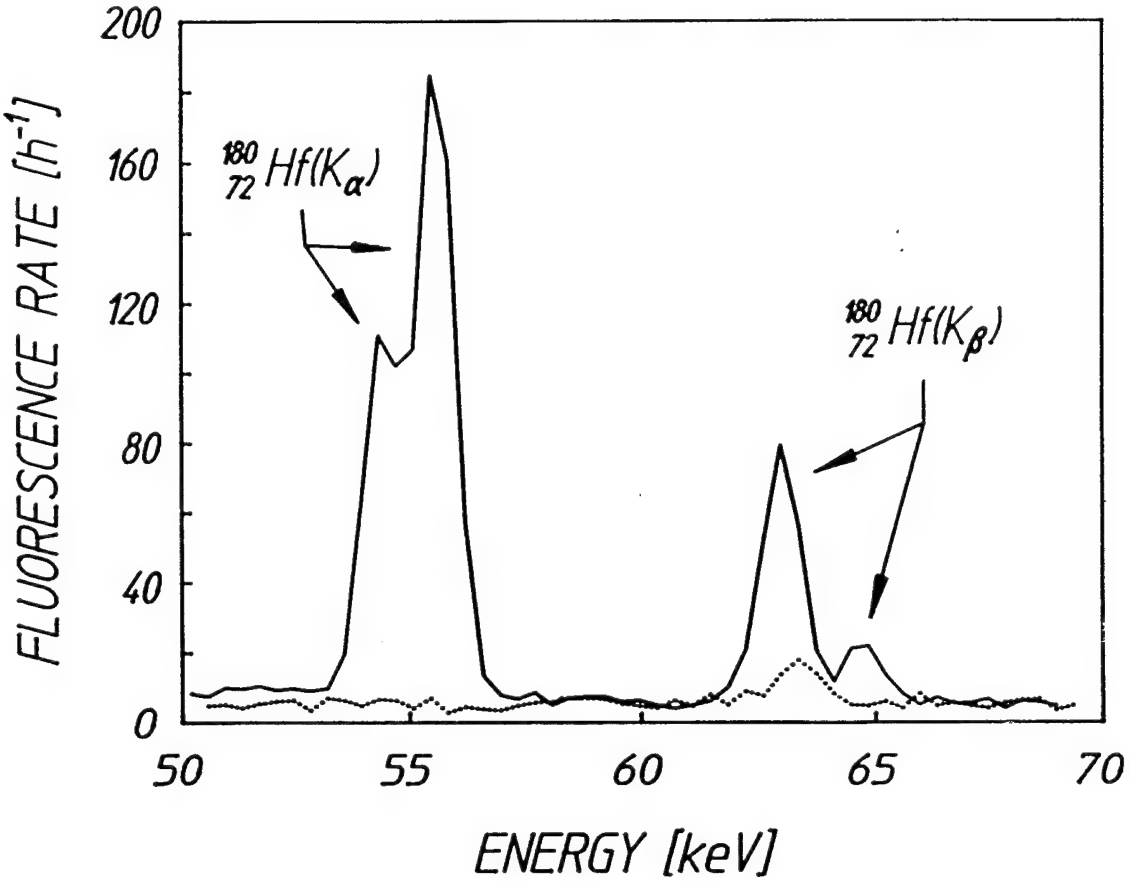
200
160
120
80
40
0
FLUORESCENCE RATE [h⁻¹]
180 72 Hf(Kα)
180 72 Hf(Kβ)
50
55
60
65
70
ENERGY [keV]

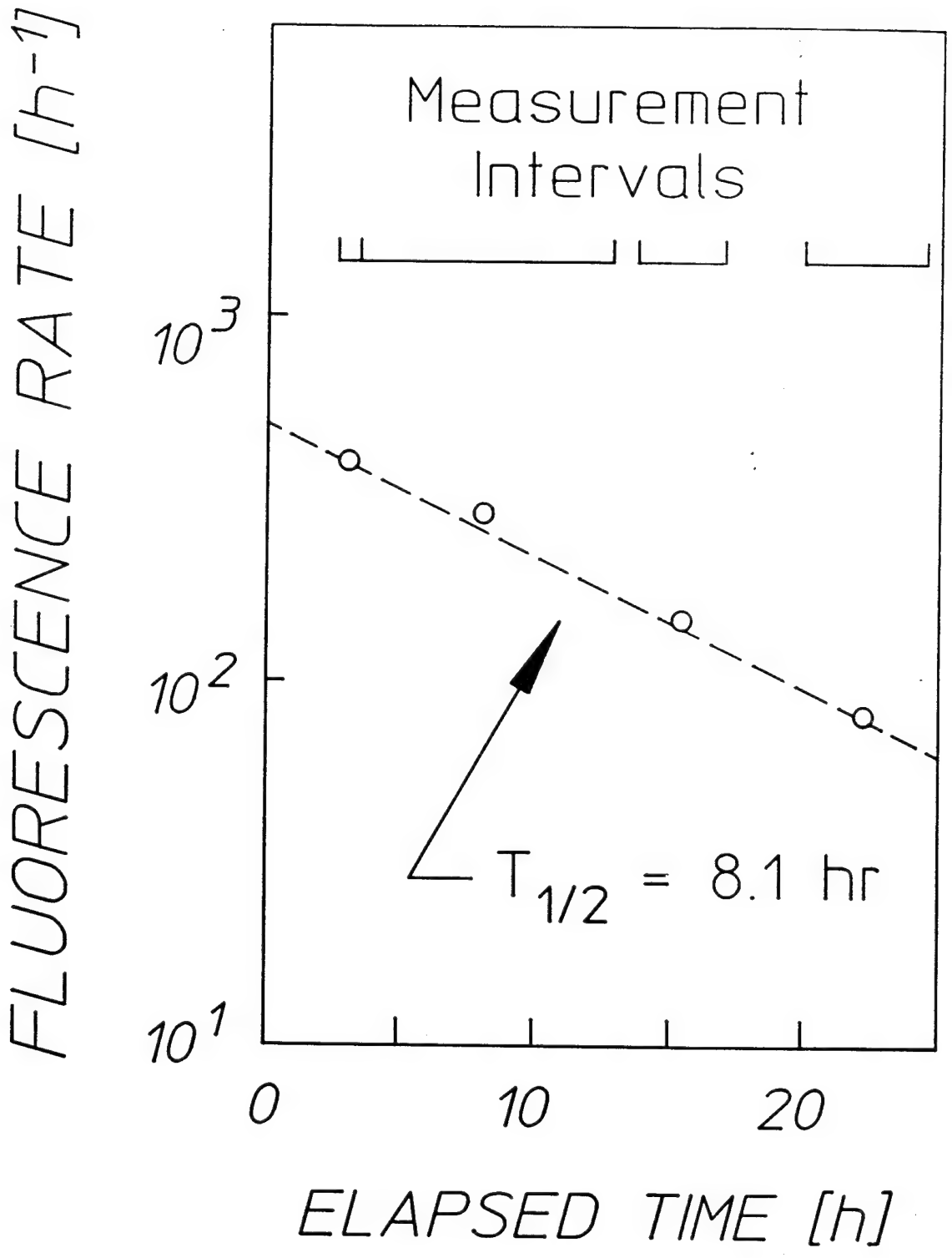
Measurement
Intervals
FLUORESCENCE RATE [h-1]
10^3
10^2
10^1
T1/2 = 8.1 hr
0
10
20
ELAPSED TIME [h]

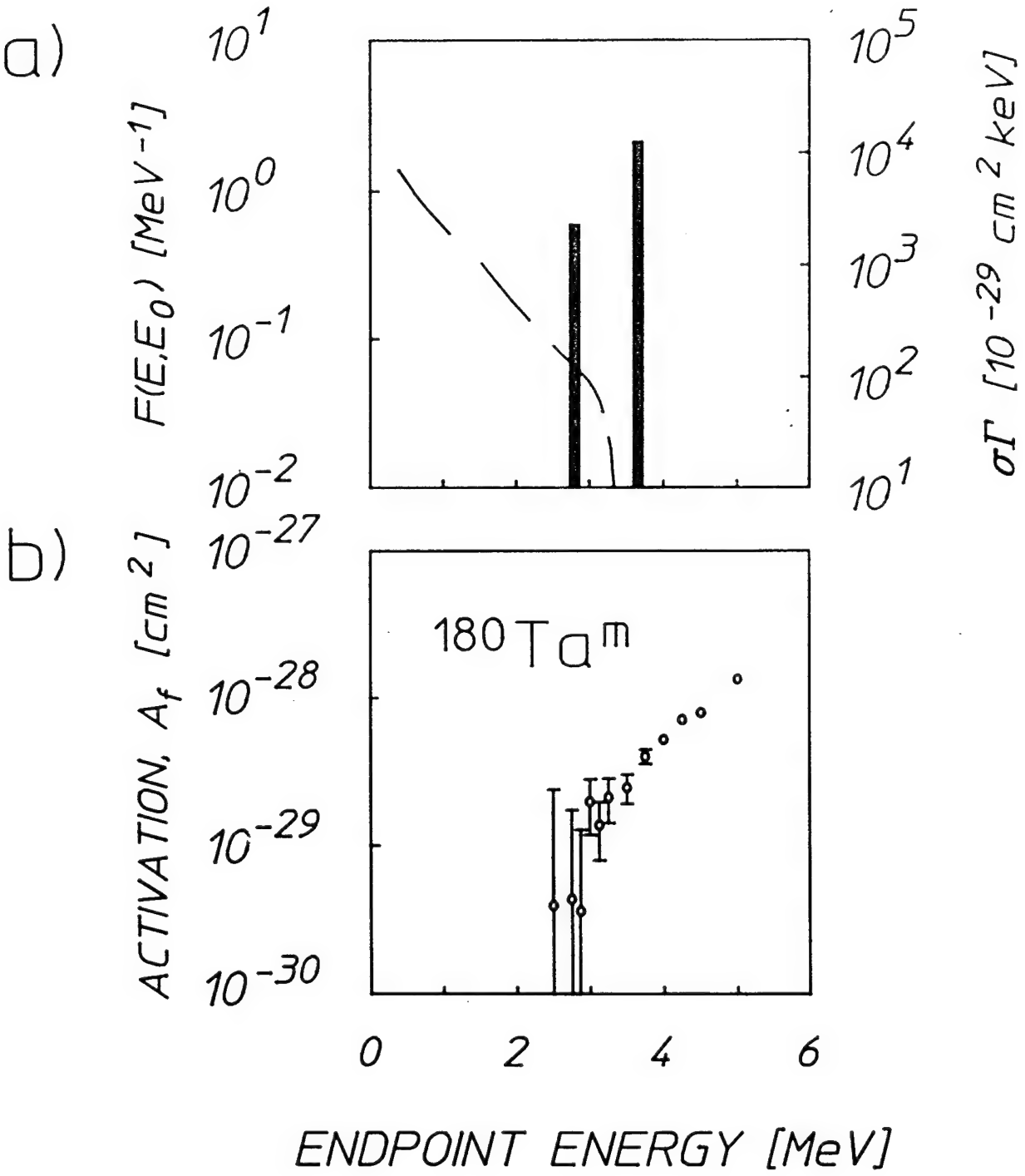
a)
b)
10^1
10^0
10^{-1}
10^{-2}
$F(E,E_0)$ [MeV^{-1}]
10^5
10^4
10^3
10^2
10^1
$\sigma\Gamma$ [10^{-29} cm^2 keV]
10^{-27}
10^{-28}
10^{-29}
10^{-30}
ACTIVATION, A_f [cm^2]
180 Ta^m
0
2
4
6
ENDPOINT ENERGY [MeV]

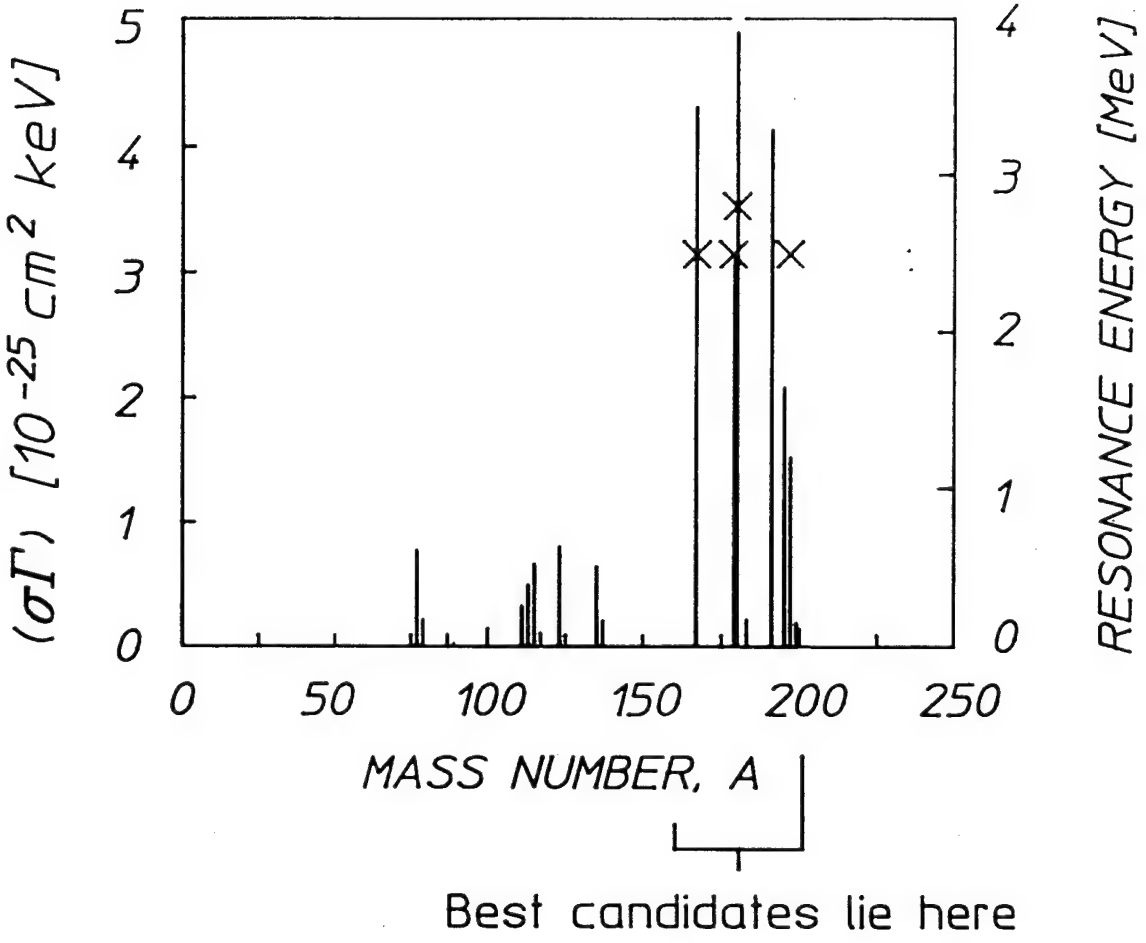
(σΓ) [10^-25 cm^2 keV]
RESONANCE ENERGY [MeV]
0
1
2
3
4
5
0
50
100
150
200
250
MASS NUMBER, A
Best candidates lie here

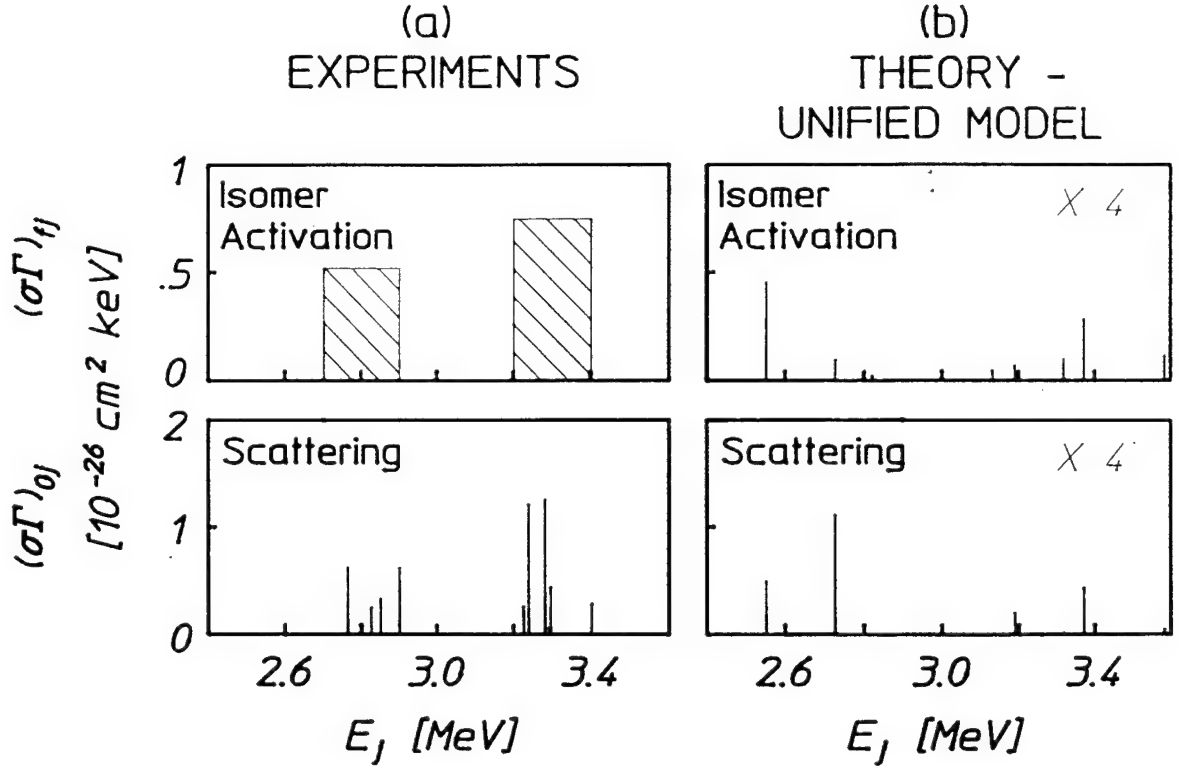
(a)
EXPERIMENTS
(b)
THEORY -
UNIFIED MODEL
Isomer
Activation
Isomer
Activation
X 4
Scattering
Scattering
X 4
1
.5
0
2
1
0
2.6
3.0
3.4
2.6
3.0
3.4
E_J [MeV]
E_J [MeV]
$(\sigma\Gamma)_{fj}$
$(\sigma\Gamma)_{0j}$
$[10^{-26}\ cm^2\ keV]$

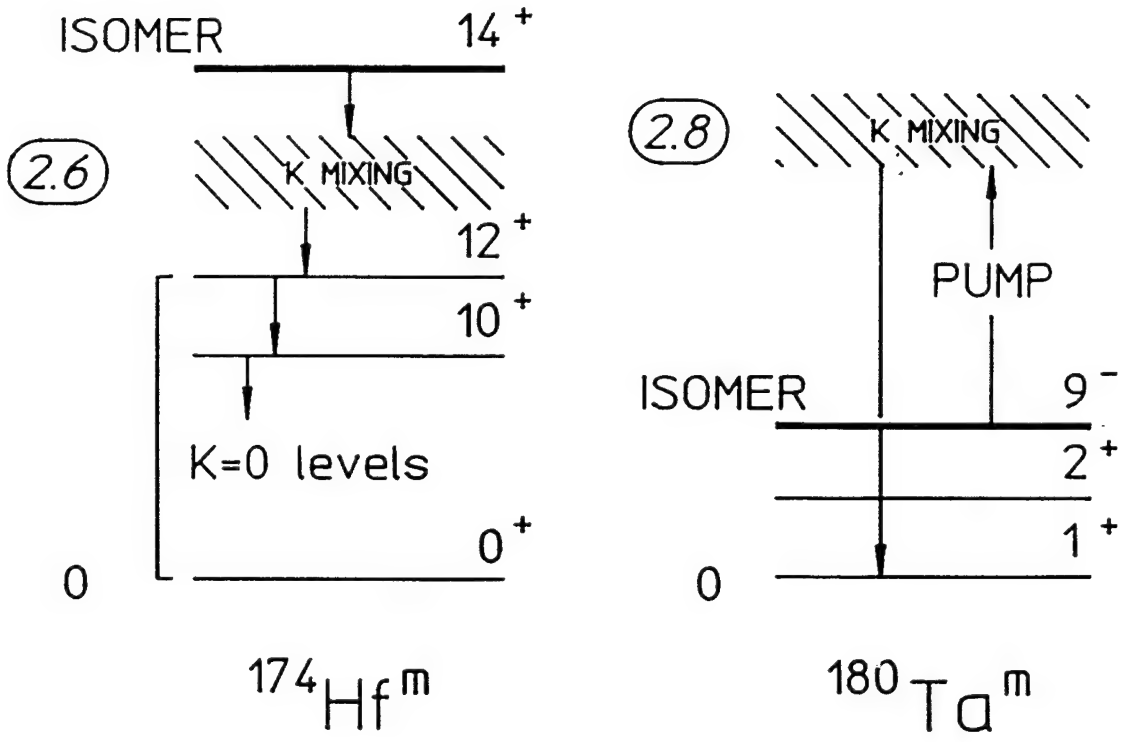
ISOMER
14 +
2.6
K MIXING
12 +
10 +
K=0 levels
0 +
0
174 Hf m
2.8
K MIXING
PUMP
ISOMER
9 -
2 +
1 +
0
180 Ta m

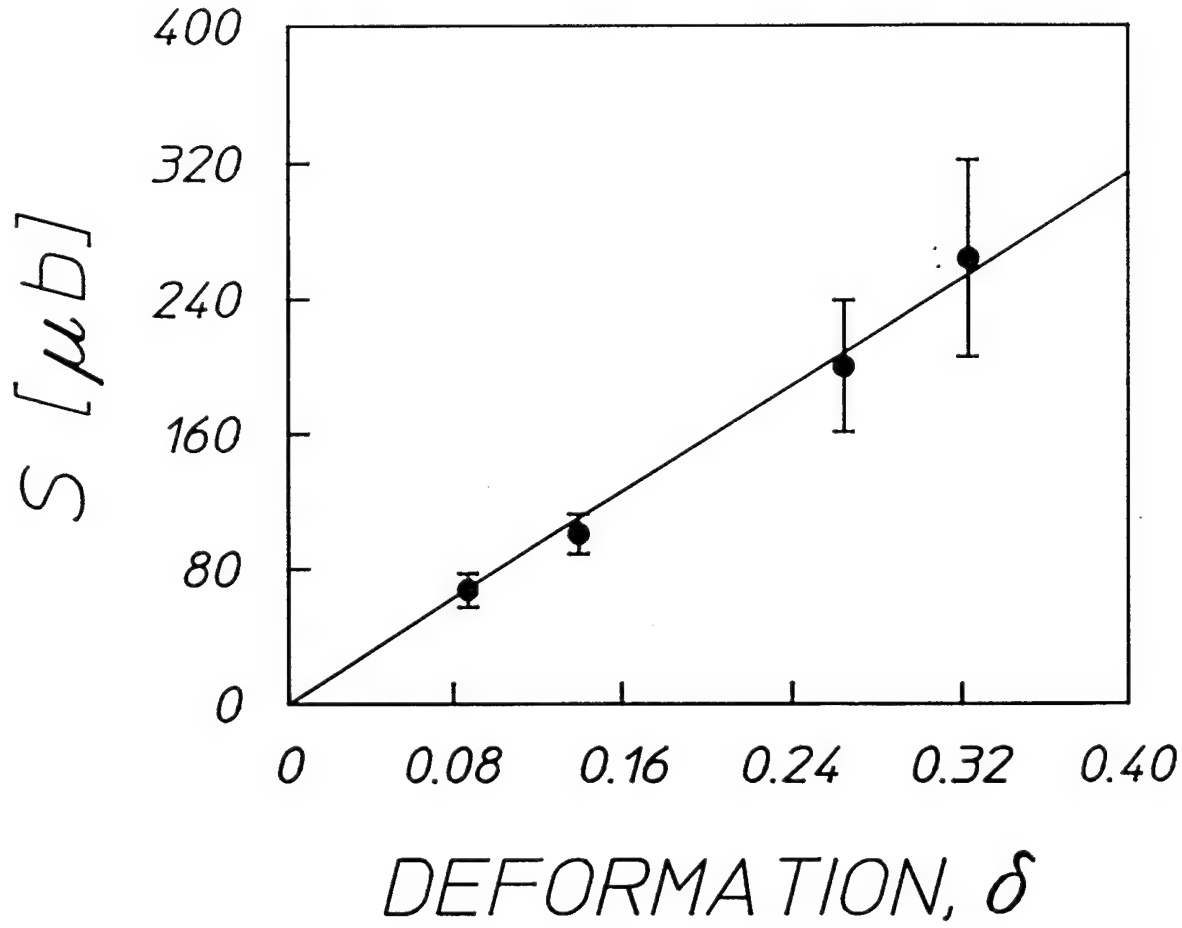
400
320
240
160
80
0
S [μb]
0
0.08
0.16
0.24
0.32
0.40
DEFORMATION, δ

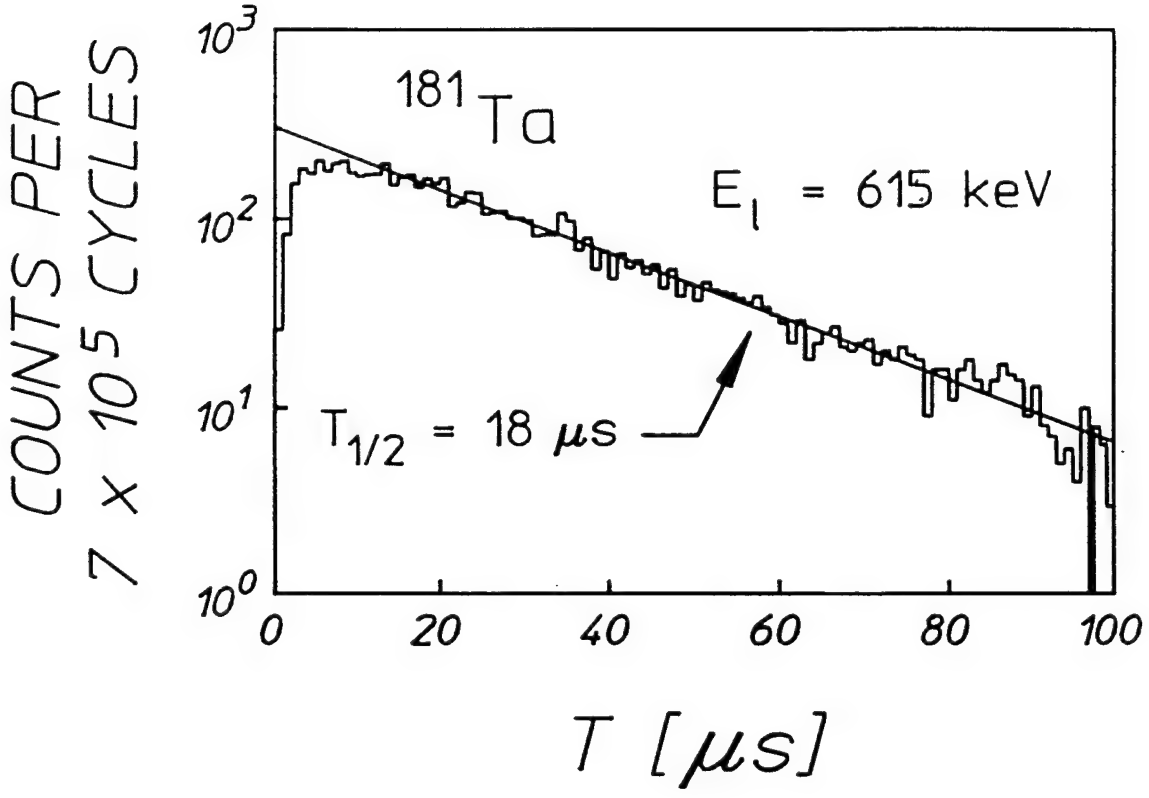
COUNTS PER
7 X 10^5 CYCLES
10^3
10^2
10^1
10^0
181 Ta
E_l = 615 keV
T_1/2 = 18 μs
0
20
40
60
80
100
T [μs]

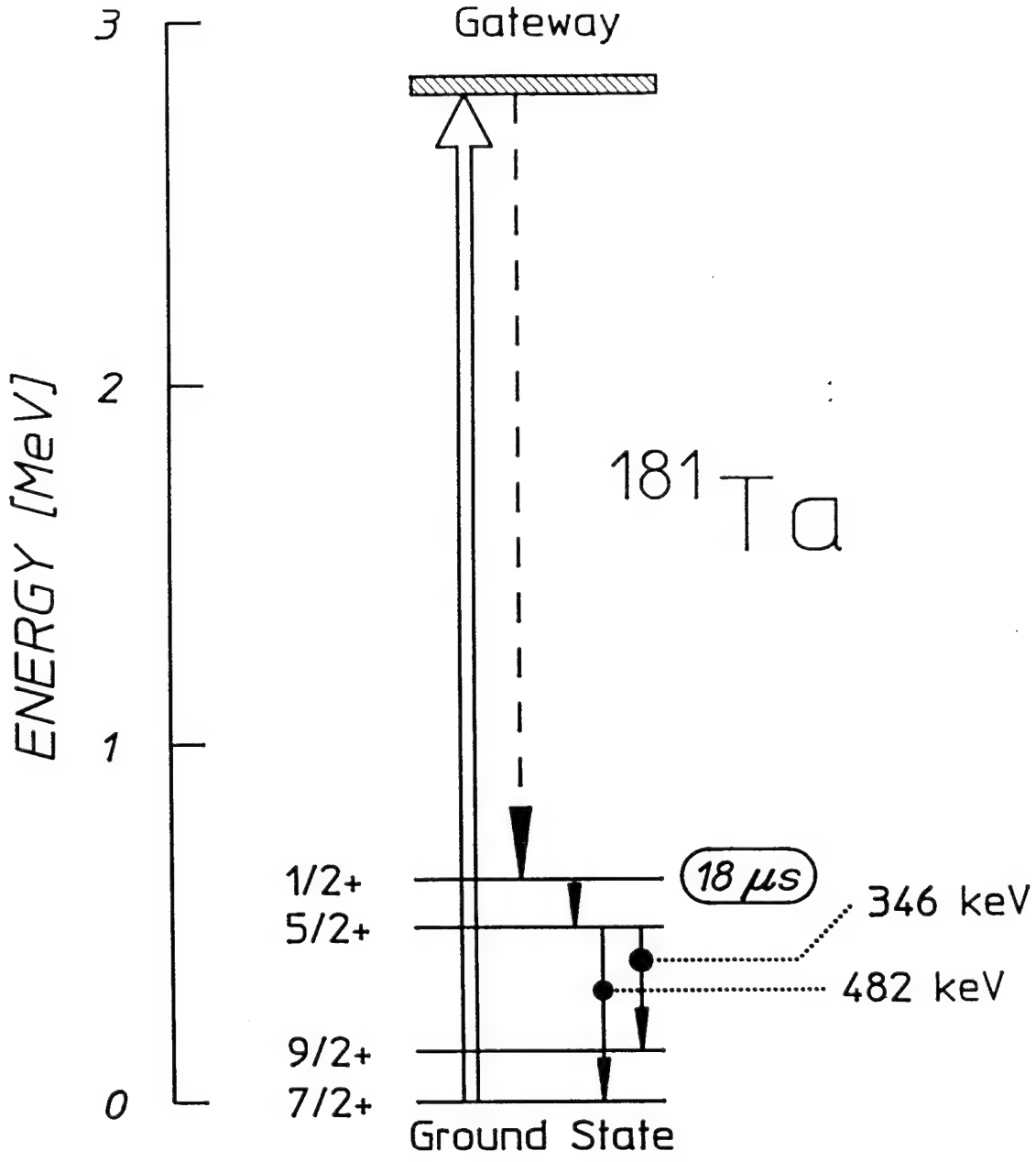
3
2
1
0
ENERGY [MeV]
Gateway
181Ta
1/2+
5/2+
9/2+
7/2+
18 μs
346 keV
482 keV
Ground State

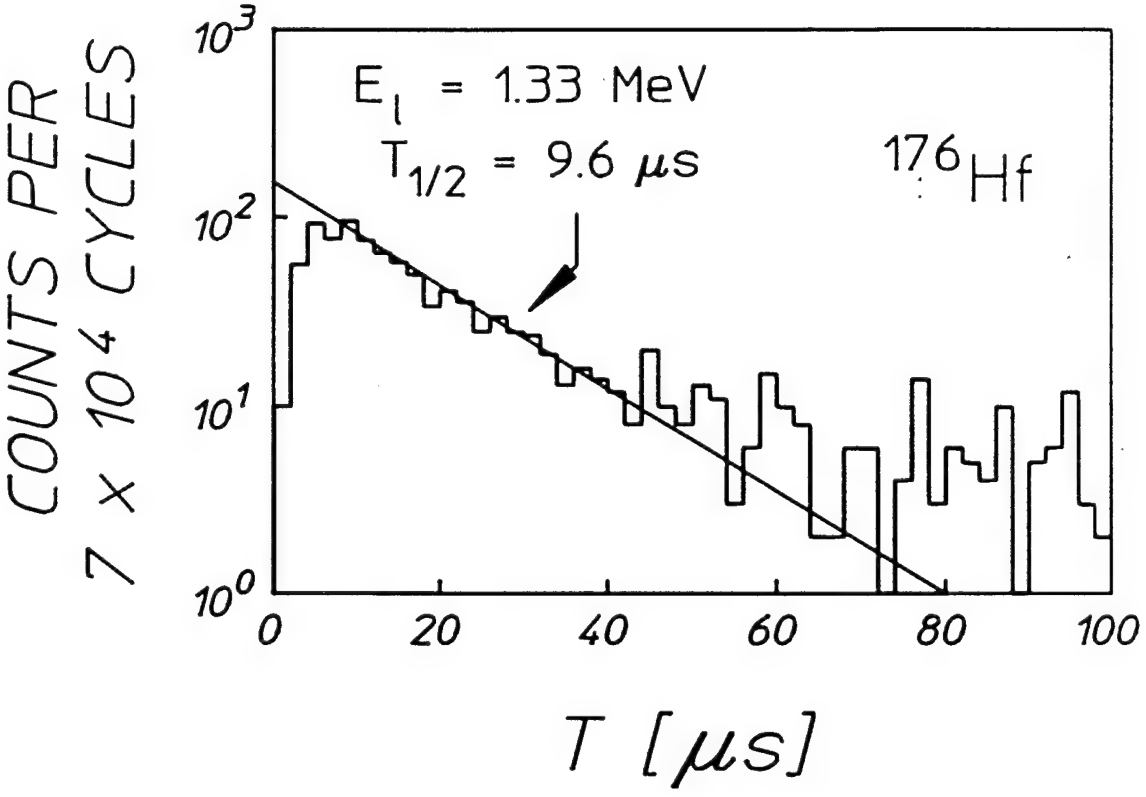
COUNTS PER
7 X 10⁴ CYCLES
10³
10²
10¹
10⁰
E_l = 1.33 MeV
T_1/2 = 9.6 μs
176Hf
0
20
40
60
80
100
T [μs]

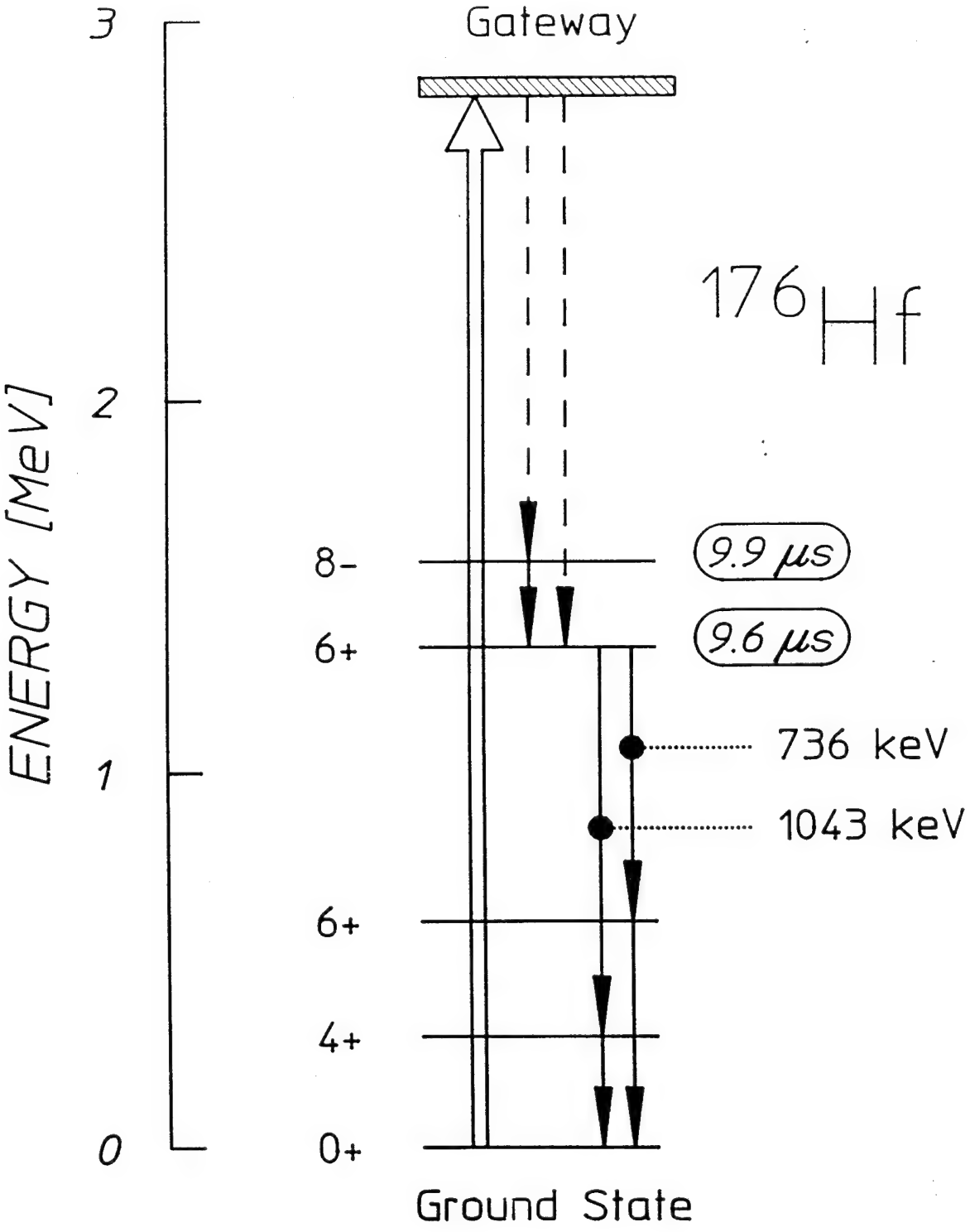
Gateway
3
2
1
0
ENERGY [MeV]
176Hf
8-
9.9 μs
6+
9.6 μs
736 keV
1043 keV
6+
4+
0+
Ground State

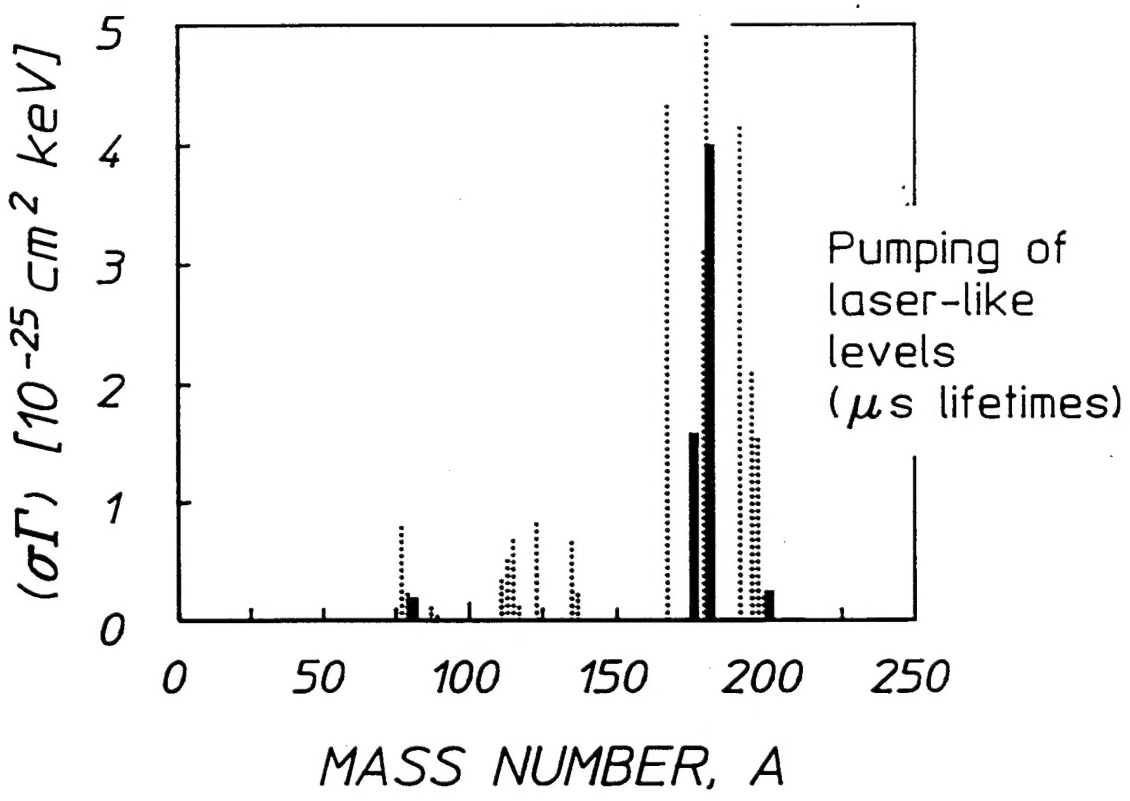
$(\sigma\Gamma)$ [10^{-25} cm^2 keV]
0
1
2
3
4
5
0
50
100
150
200
250
MASS NUMBER, A
Pumping of
laser-like
levels
(μs lifetimes)

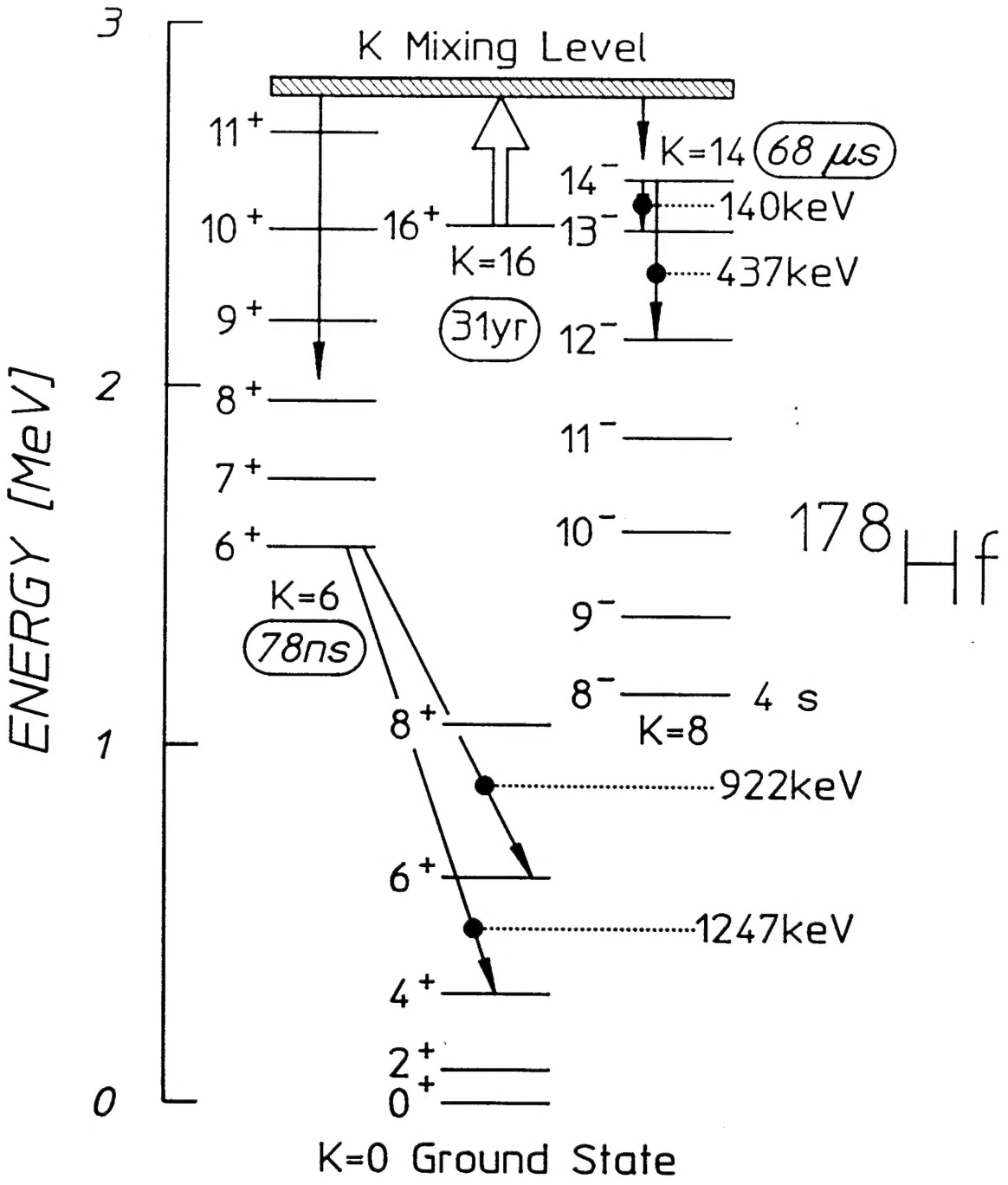
K Mixing Level
11+
10+
16+
9+
8+
7+
6+
K=16
31yr
K=6
78ns
K=14
68 μs
14−
13−
12−
11−
10−
9−
8−
140keV
437keV
4 s
K=8
922keV
1247keV
8+
6+
4+
2+
0+
178Hf
ENERGY [MeV]
3
2
1
0
K=0 Ground State

II. Index of Technical Reports

"Basic Study of the Pumping of a Gamma-Ray Laser," by C. B. Collins, First Annual Technical Report GRL/9401, NRL Contract No. N00014-93-K-2005.

"Basic Study of the Pumping of a Gamma-Ray Laser," by C. B. Collins, Second Annual Technical Report GRL/9501, NRL Contract No. N00014-93-K-2005.

III. Index of Publications

"Quantum Interference Asymmetries in the Mössbauer Spectrum of ^{57}Fe Induced by Radiofrequency Maagnetic Fields," by S. Olariu, T. W. Sinor, and C. B. Collins, Phys. Rev. B 50, 43-51 (1994).

"Low Energy Conversion Electron Mössbauer Spectroscopy Using a Chevron Microchannel Plate Detector," by T. W. Sinor, J. D. Standifird, K. N. Taylor, C. Hong, J. J. Carroll, and C. B. Collins, Rev. Sci. Instrum. 64, 2570-2573 (1993).

"Absolute Calibration of Low Energy, Thick Target Bremsstrahlung," by P. von Neumann-Cosel, N. Huxel, A. Richter, C. Spieler, J. J. Carroll, and C. B. Collins, Nucl. Instrum Meth. A338, 425-431 (1994).

"Intermediate Structure in the Photoexcitation of $^{77}Se^{m}$, $^{79}Br^{m}$ and $^{137}Ba^{m}$," by J. J. Carroll, C. B. Collins, K. Heyde, M. Huber, P. von Neumann-Cosel, V. Yu. Ponomarov, D. G. Richmond, A. Richter, C. Schlegel, T. W. Sinor, and K. N. Taylor, Phys. Rev. C 48, 2238-2245 (1993).

"Mössbauer Effect Measurement of the Recoil-free Fraction for ^{57}Fe Implanted in a Nanophase Diamond Film," by T. W. Sinor, J. D. Standifird, F. Davanloo, K. N. Taylor, C. Hong, J. J. Carroll, and C. B. Collins, Appl. Phys. Lett. 64, 1221-1223 (1994).

"Evidence for Nuclear Multiphoton Transitions in ^{57}Fe Based on Radio-frequency Sidebands to the Forbidden Hyperfine Components of the 14.4 keV Transition," S. Olariu, T. W. Sinor, and C. B. Collins, Phys. Rev. B 50, 616-618 (1994).

"Progress in the Pumping of a Gamma-Ray Laser," by C. B. Collins and J. J. Carroll, Int. J. Laser Phys. 5, 209-230 (1995).

"K Mixing in $^{178}Hf^{m}$," by C. B. Collins, J. J. Carroll, Yu. Ts. Oganessian, and S. A. Karmamian, Int. J. Laser Phys. 5, 280-283 (1995).